Vol. **8**, **4**, 351-385 (2001)

**Archives of Computational Methods in Engineering**
*State of the art reviews*

# Topology Optimization of Elastic Continua Using Restriction

T. Borrvall

Division of Mechanics, Mechanical Engineering Systems
Linköping University
SE-581 83 Linköping, Sweden

## Summary

This is a study of restriction methods in topology optimization of linear elastic continua. An ill-posed optimization problem is transformed into a well-posed one by restricting the feasible set, hence the term restriction. A number of restriction methods are presented and compared, of which some have been treated previously in the literature and some are new. Advantages and drawbacks of the methods are discussed from a theoretical as well as a numerical point of view. The problems of minimizing compliance and designing compliant mechanisms constitute the base for these discussions and several numerical examples are presented that illustrate features of the various restriction methods.

## 1 INTRODUCTION

Structural optimization is usually divided into the three subfields size, shape and topology optimization. The latter, sometimes called layout optimization, is by far the most general as the connectedness of the optimal structure is not assumed a priori as it is in both size and shape optimization. It is known that the topology of a mechanical structure decisively influences its performance, hence it is important to deal with these kind of problems. For a comprehensive review of the field, refer to the monographs by Bendsøe [1] and Hassani and Hinton [2] or to the review article by Rozvany *et al.* [3].

In topology optimization of linear elastic continua, a naive mathematical modelling of the physical situation results in an ill-posed optimization problem. Typically the problem is posed in terms of distributing a fixed isotropic material in a fixed domain so that every domain point is associated with either material or void. This determines a feasible set that lacks closure and in general the infimum cannot be attained at any feasible point. A partly relaxed version of the compliance minimization problem was first solved by Bendsøe and Kikuchi [4]. They extend the feasible set to include a periodic microstructure with rectangular inclusion from which the effective stiffness is determined by homogenization formulae. To obtain a well-posed optimization problem however, a full relaxation is required [5]. This is equivalent to extending the feasible set to include all the microstructures made from material and void, i.e. to form the G-closure [6, 7] of the feasible set. Unfortunately, the G-closure is not explicitely known in linear elasticity [8] and the relaxed problem seems in general difficult to solve. In the special case of compliance, it is sufficient to extend the feasible set to consist of only sequential laminates, a subset of the G-closure. The relaxed compliance minimization problem has been solved in this way by Allaire and Kohn [8], Bendsøe *et al.* [9] and Allaire *et al.* [10]. This approach relies heavily on the fact that for a given volume fraction, the sequential laminates attain the optimal bounds on the effective stiffness of an arbitrary microstructure, see for instance Allaire and Kohn [11]. For another objective, it seems that new optimal microstructures need to be established before the relaxed problem can be explicitely solved. Even when the relaxed problem can be solved, the optimal structure is probably difficult and expensive to manufacture because of the complex material. To avoid this, the structural fluctuations can be kept on a finite scale by

 ISSN: 1134–3060 Received: May 2001

restricting the feasible set to a closed subset. No microstructures are introduced and the optimal structures are relatively simple, hence easy and cheap to manufacture. Besides a (hopefully slight) reduction in performance of an optimal structure, a main drawback with a restriction approach is that the numerical treatment is challenging due to non-convexity of the optimization problem. The significance of this drawback depends on how the restriction is performed which motivates a systematic investigation of *restriction methods* in topology optimization of linear elastic continua.

Up to now, the most popular problem in topology optimization of linear elastic continua is the problem of minimizing compliance. This problem has nice features that have been taken advantage of in the literature, see for instance [8, 10, 12, 13], and has also been extended to non-linear constitutive models [14, 15, 16]. The problem of designing compliant mechanisms was introduced by Ananthasuresh *et al.* [17] and has proved a challenging as well as a popular problem. A compliant mechanism is not a mechanism in the rigid-body sense, but a structure that achieve motion from the flexibility of some or all of its structural members. The advantages with a compliant mechanism in comparison to a conventional rigid-body mechanism include the possibility of single-piece construction and the reduction of friction, wear, backlash and noise [18].

The main objective for a compliant mechanism is to perform useful work on a workpiece, an objective that has resulted in varying mathematical formulations in the literature. Frecker *et al.* [19] and Nishiwaki *et al.* [20] formulate it in terms of maximizing the ratio of mutual potential energy to strain energy, and in Hetrick and Kota [21] an energy formulation is used where the objective is to maximize the mechanical efficiency. In Larsen *et al.* [22] the user is allowed to specify the mechanical and geometrical advantages of the compliant mechanism, and in Sigmund [23] the mechanical advantage is maximized. This paper follows the latter reference in the sense that the objective is to transmit an applied force in to a maximal force on an elastic workpiece. The linear elasticity assumption is here questionable, see [23], but since the objective with this paper is to investigate restriction methods rather than the mathematical modelling of structural behaviour, this is disregarded. For design of compliant mechanisms where non-linear effects are taken into account, the reader is referred to [24, 25]. Compliant mechanism design is an example of a topology optimization problem for which solving the relaxation can be a cumbersome task, hence a restriction method is to prefer.

A compliant mechanism is in general categorized as a lumped or distributed compliant mechanism. For a lumped compliant mechanism, the elastic deformation is concentrated to a finite number of flexural pivots. Disadvantages with lumped compliance include high stress concentrations and manufacturing difficulties [18]. Considering that compliant mechanisms are often used in the field of MEMS (MicroElectroMechanical Systems), the manufacturing issue is highly important [22]. The mechanism should possess distributed compliance which means that the flexibility is distributed almost equally throughout the mechanism. No structural part is much thinner than any other which eliminates the drawbacks with lumped compliance. Some restriction methods in this paper exclude the possibility for lumped compliance regions to occur and are therefore suitable for the design of distributed compliant mechanisms.

The rest of the paper is organized as follows. In section 2, continuum formulations of the state and optimization problems are given for the purpose of discussing existence issues. Section 3 presents some test problems that are used for evaluating the different restriction methods. In section 4, the problems in section 2 are finite element discretized and numerical issues are discussed. Sections 5-7 are devoted to restriction methods categorized as follows, finite dimensional set of designs (section 5), bounds on the design gradient (section 6) and filters (section 7). Section 8 discusses other types of restriction methods and the paper ends with some discussions and conclusions in section 9.

## 2 PROBLEM FORMULATIONS

This section starts with the description of the equation that determines the state of equilibrium of a structure in contact with a workpiece. This equation is used when formulating the two optimization problems that will be the base for evaluating the restriction methods. Some notations that may be different from the usual are first presented. A geometric vector is written in **bold-face** and $|\cdot|$ denotes the euclidean norm of such a vector. Assuming that the $L^p$-spaces, $1 \leq p \leq \infty$, are familiar to the reader, $\boldsymbol{L}^p$ denotes the space of vector valued functions for which the euclidean norm belongs to $L^p$. The norm is in either case denoted $\|\cdot\|_p$. Furthermore, the space $\boldsymbol{H}^1$ is the Sobolev space of vector valued functions for which the function itself and its gradient are vector and tensor valued functions respectively with square integrable norms. The norm on this space is denoted $\|\cdot\|_{\boldsymbol{H}^1}$. For details on Sobolev spaces, the reader is referred to [26].

### 2.1 The State Problem

Let the *structural domain* $\Omega \subset \boldsymbol{R}^d$ * be an open, bounded and connected set with a Lipschitzian boundary $\Gamma$, see Figure 1. Furthermore, let $\Gamma_u \subset \Gamma$, $|\Gamma_u| > 0$, be the part of the boundary where displacements are fixed, and $\Gamma_t = \Gamma \setminus \Gamma_u$ the part where tractions are prescribed. The tractions are represented by a vector field $\boldsymbol{t} \in \boldsymbol{L}^2(\Gamma_t)$. The fourth order tensor $\boldsymbol{E}$ represents an appropriately chosen isotropic material and $\rho \in L^\infty(\Omega)$ is a density that for some $0 < \rho_\epsilon \ll 1$ fulfils $\rho_\epsilon \leq \rho \leq 1$ a.e. in $\Omega$. It is assumed that $\boldsymbol{E}$ satisfies the usual symmetry , ellipticity and boundedness features. Let $f_q$, $q \geq 1$, be a parameterizable function on $[\rho_\epsilon, 1]$ with range $(0, 1]$, in this context known as a *material interpolation function* This function should satisfy some requirements that will be apparent throughout this section. The structure is represented by the effective elasticity tensor $\boldsymbol{E}_q(\rho) = f_q(\rho)\boldsymbol{E}$ and occupies the entire structural domain. The material interpolation function $f_q$ should be chosen so that the points in $\Omega$ where $\rho = 1$ are occupied with the material represented by the tensor $\boldsymbol{E}$, i.e. $f_q(1) = 1$. Moreover, the points in $\Omega$ where $\rho = \rho_\epsilon$ should be occupied with a very compliant material intended to represent void, which indicates that $f_q$ should fulfil $f_q(\rho_\epsilon) \ll 1$. In between $\rho_\epsilon$ and 1, $f_q$ should be increasing in order to assure that increasing the density means increasing the stiffness.

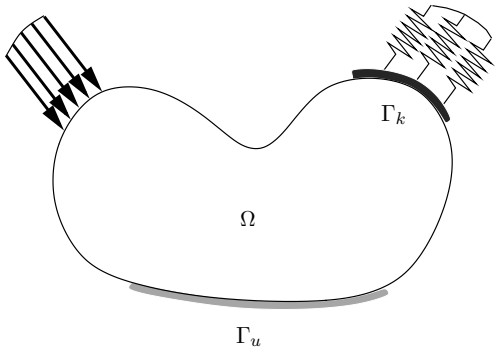


**Figure 1.** A structural domain for the state problem in 2 dimensions

*For the sake of generality, the space dimension $d$ may in section 2 be considered arbitrary (which in practice means $d = 2$ or $d = 3$). However, because of the chosen numerical examples and to keep the exposition and notation simple, it will from section 3 and on be assumed that $d = 2$. It should nevertheless be mentioned that everything can be generalized to include the case $d = 3$.

Now the set $\Gamma_k \subset \Gamma_t$ is introduced where the structure can interact with some elastic workpiece. The stiffness of this workpiece is represented by a vector field $\boldsymbol{k} \in \boldsymbol{L}^\infty(\Gamma_k)$ so that for a structural displacement field $\boldsymbol{v}$, the force that is exerted on the structure by the workpiece is equal to

$$\boldsymbol{t}_k(\boldsymbol{v}) = -(\boldsymbol{k} \cdot \boldsymbol{v})\frac{\boldsymbol{k}}{k}.$$

It is here assumed that $k = |\boldsymbol{k}| > 0$ on $\Gamma_k$.

The space of kinematically admissible displacements, $\boldsymbol{V}$, is the closed subspace of $\boldsymbol{H}^1(\Omega)$ whose members are such that their traces vanish on $\Gamma_u$. On $\boldsymbol{V}$, Cauchy's infinitesimal strain tensor is given by

$$\boldsymbol{\epsilon}(\boldsymbol{v}) = \frac{1}{2}(\nabla \boldsymbol{v} + \nabla \boldsymbol{v}^T).$$

For a given material interpolation function $f_q$, the internal work symmetric bilinear form on $\boldsymbol{V} \times \boldsymbol{V}$ is defined as

$$a_{\rho,k}(\boldsymbol{u}, \boldsymbol{v}) = a_\rho(\boldsymbol{u}, \boldsymbol{v}) + a_k(\boldsymbol{u}, \boldsymbol{v})$$

where

$$a_\rho(\boldsymbol{u}, \boldsymbol{v}) = \int_\Omega \boldsymbol{\epsilon}(\boldsymbol{u}) \cdot \boldsymbol{E}_q(\rho) \cdot \boldsymbol{\epsilon}(\boldsymbol{v})$$

and

$$a_k(\boldsymbol{u}, \boldsymbol{v}) = \int_{\Gamma_k} \frac{1}{k}(\boldsymbol{k} \cdot \boldsymbol{u})(\boldsymbol{k} \cdot \boldsymbol{v}). \tag{1}$$

For any $\rho$ satisfying the requirements mentioned above, the following relations hold,

$$|a_{\rho,k}(\boldsymbol{u}, \boldsymbol{v})| \leq M \|\boldsymbol{u}\|_{\boldsymbol{H}^1(\Omega)} \|\boldsymbol{v}\|_{\boldsymbol{H}^1(\Omega)}, \quad \forall \boldsymbol{u}, \boldsymbol{v} \in \boldsymbol{V}$$

and

$$a_{\rho,k}(\boldsymbol{v}, \boldsymbol{v}) \geq f_q(\rho_\epsilon)\alpha \|\boldsymbol{v}\|^2_{\boldsymbol{H}^1(\Omega)}, \quad \forall \boldsymbol{v} \in \boldsymbol{V}$$

for some strictly positive constants $\alpha$ and $M$. It is crucial that the parameter $\rho_\epsilon$ is strictly positive to assure ellipticity of the operator $a_{\rho,k}$. The external load linear form, $\ell$, is defined as

$$\ell(\boldsymbol{v}) = \int_{\Gamma_t} \boldsymbol{t} \cdot \boldsymbol{v}, \tag{2}$$

which makes it a bounded linear functional on $\boldsymbol{V}$. The total potential energy of the system, i.e. the structure, the workpiece and the external loads, can now be stated as

$$\mathcal{J}(\rho, \boldsymbol{v}) = \frac{1}{2}a_{\rho,k}(\boldsymbol{v}, \boldsymbol{v}) - \ell(\boldsymbol{v}).$$

The equilibrium displacement field is the unique minimizer of $\boldsymbol{v} \mapsto \mathcal{J}(\rho, \boldsymbol{v})$, also characterized as the solution to the following variational equality

$$\boldsymbol{u} \in \boldsymbol{V}: \quad a_{\rho,k}(\boldsymbol{u}, \boldsymbol{v}) = \ell(\boldsymbol{v}), \quad \forall \boldsymbol{v} \in \boldsymbol{V}. \tag{3}$$

These two formulations are the well known principles of minimum potential energy and virtual work.

## 2.2 The Optimization Problems

Here it is assumed that an appropriate material interpolation function $f_q$ has been chosen, given by for instance (4) or (5). The intention is to present the optimization problems in nested form, where the state variable $\boldsymbol{u}$ is eliminated through (3). For a given density $\rho$ (again satisfying the requirements mentioned in the previous section), the unique solution to (3) is denoted $\boldsymbol{u}(\rho)$.

The *compliance* of the structure is an inverse measure of the stiffness and is mathematically seen as a function of $\rho$. It is denoted $\tilde{\ell}$ and given by $\tilde{\ell}(\rho) := \ell(\boldsymbol{u}(\rho))$, where $\ell$ is given by (2). Furthermore, the force that is exerted on the structure by the workpiece is projected in the $\boldsymbol{k}/k$ direction and integrated on $\Gamma_k$,

$$t_k(\boldsymbol{v}) = \int_{\Gamma_k} \boldsymbol{t}_k(\boldsymbol{v}) \cdot \frac{\boldsymbol{k}}{k} = -\int_{\Gamma_k} (\boldsymbol{k} \cdot \boldsymbol{v})(\frac{\boldsymbol{k}}{k} \cdot \frac{\boldsymbol{k}}{k}) = -\int_{\Gamma_k} (\boldsymbol{k} \cdot \boldsymbol{v}).$$

Again the displacement field is eliminated through (3) and $\tilde{t}_k$ is viewed as a function of $\rho$, i.e. $\tilde{t}_k(\rho) := t_k(\boldsymbol{u}(\rho))$. This function can be seen as a scalar measure of the total force that is exerted on the workpiece by the structure or vice versa, a large negative value of $\tilde{t}_k$ means that a large force is exerted on the workpiece by the structure. On the other hand, a large positive value of $\tilde{t}_k$ should in one sense be prohibited since that would mean that the structure and workpiece are separated. Because of the proposed model, which could be seen as a very simple frictionless bilateral contact model, this is not the case. Nevertheless, the objective will be to minimize $\tilde{t}_k$ and a positive value will thus never occur in practice. The direction $\boldsymbol{k}/k$ is chosen as the desired direction of a force exerted by the structure on a workpiece and $k$ measures the stiffness of this workpiece in this direction.

### *2.2.1 Maximum stiffness design*

The first problem to consider is the problem of maximizing stiffness subject to a constraint on the volume. Here $\Gamma_k = \emptyset$ and the problem can be formulated mathematically as

$$(\boldsymbol{P})_{\text{stiff}} \quad \begin{cases} \min\limits_{\rho} & \tilde{\ell}(\rho) \\ \text{s.t.} & \int_\Omega \rho \le \overline{V} \\ & \rho_\epsilon \le \rho \le 1 \quad \text{a.e. in } \Omega. \end{cases}$$

### *2.2.2 Compliant mechanism design*

The second problem that is considered is to design a compliant mechanism. The objective is to maximize the force that is exerted on the workpiece by the structure. Following [23], a volume constraint is introduced in order to keep a low volume fraction for manufacturing reasons, as well as a constraint on the compliance in order to keep the stresses in the structure low. In fact, in [23] the constraint is put on the input displacement in the direction of the applied point load. A generalization of this constrain to the case of an arbitrary line (or surface) load would be a constraint on the compliance. This is further motivated by consulting [9] where it is demonstrated that the integrated von Mises equivalent stress is bounded by some constant times the integrated strain energy density which here is a smaller quantity than the compliance. This does not imply that the stresses are uniformly bounded pointwise but it is demonstrated in [23] that there is reason to believe that they are. The problem can now be formulated mathematically as

$$(\boldsymbol{P})_{\text{mech}} \quad \begin{cases} \min\limits_{\rho} & \tilde{t}_k(\rho) \\ \text{s.t.} & \int_\Omega \rho \le \overline{V} \\ & \tilde{\ell}(\rho) \le \overline{\ell} \\ & \rho_\epsilon \le \rho \le 1 \quad \text{a.e. in } \Omega. \end{cases}$$

### 2.3 Penalty Schemes

In topology optimization, a goal is to assure that an optimal density $\rho^*$ to either one of the optimization problems $(\boldsymbol{P})_{\text{stiff}}$ or $(\boldsymbol{P})_{\text{mech}}$ is discrete valued. This means that $\rho^*$ should preferrably take only the values $\rho_\epsilon$ or 1 almost everywhere in $\Omega$. This could be explicitely imposed when formulating the problem by changing the last constraint in any of the problems to $\rho \in \{\rho_\epsilon, 1\}$ a.e. in $\Omega$. Alternatively, one could introduce some kind of penalization in the problem in either one of the following two ways.

One one hand, one could choose the material interpolation function so that intermediate density values are given a higher cost compared to discrete density values. Consider for instance

$$f_q(\rho) = \rho^q, \tag{4}$$

commonly known as the SIMP (Solid Isotropic Material with Penalization) interpolation function [27, 28], or

$$f_q(\rho) = \frac{\rho}{1 + (q-1)(1-\rho)}, \tag{5}$$

another SIMP variant [29]. It is seen that $f_1(\rho) = \rho$ and that $f_q(\rho)$ decreases towards 0 as $q$ increases for an intermediate density value $\rho$. For high $q$, the intermediate density values are suppressed as they contribute comparatively little to the stiffness. The parameter $q$ is intended to be used as a control of the level of penalization, as a high value of $q$ implies hard penalization. For examples of other artificial material interpolation schemes, see for instance [30, 31], and for a general treatment of material interpolation schemes in topology optimization the reader is referred to [32].

Another way is to choose the material interpolation function $f_q(\rho) = \rho$ and explicitely penalize the intermediate values by adding a penalty term in the objective of the form $QP(\rho)$, where $Q$ is a positive scalar used to find a proper degree of penalization and $P$ is a penalty function that encourages discrete valued densities. This penalty function could take the form, see for instance [33, 34 ],

$$P(\rho) = \int_\Omega (1-\rho)(\rho - \rho_\epsilon). \tag{6}$$

The intermediate density values contribute more to the objective than the discrete density values, hence they are suppressed.

### 2.4 Existence Issues

For convenience of this section and the rest of the paper, let $\mathcal{H}$ denote the densities $\rho$ that are determined by the constraints in either one of the problems $(\boldsymbol{P})_{\text{stiff}}$ or $(\boldsymbol{P})_{\text{mech}}$.

In general, the problems considered in section 2.2 are ill-posed when discrete constraints are imposed or penalization is introduced as described in the previous section. The term ill-posed in this context means that there are no optimal solutions. A sufficient condition for such an optimization problem to be well-posed is for it to have the following two properties. First, the set $\mathcal{H}$ has to be compact and second, the objective function has to be lower semi-continuous. Furthermore, since the problem is infinite dimensional, these two properties must be valid with respect to the same topology .

For the problem $(\boldsymbol{P})_{\text{stiff}}$, $\mathcal{H}$ is always weakly* compact in $L^\infty(\Omega)$ but the objective function is not known to be weakly* lower semi-continuous in $L^\infty(\Omega)$ when $q > 1$. However, it is so when $q = 1$ and hence this problem is well-posed, a problem that is known as the *variable thickness sheet problem* [35, 36]. For the problem $(\boldsymbol{P})_{\text{mech}}$, $\mathcal{H}$ is not known to be weakly* compact in $L^\infty(\Omega)$ unless $q = 1$ and the objective function is not known to be

weakly* lower semi-continuous in $L^\infty(\Omega)$ for any $q$. It appears likely that this problem is ill-posed even for $q = 1$.

Restriction is a measure for obtaining a well-posed optimization problem in this context. Starting from an ill-posed problem with a feasible set $\mathcal{H}$, the idea is to restrict this set to another set $\tilde{\mathcal{H}} \subset \mathcal{H}$ so that the problem becomes well-posed. Noting that the objective function in either one of the optimization problems $(\boldsymbol{P})_{\text{stiff}}$ or $(\boldsymbol{P})_{\text{mech}}$ is strongly (lower semi-)continuous in $L^p(\Omega)$, $1 \leq p < \infty$, the set $\tilde{\mathcal{H}}$ should be compact in the same sense. At this point, it should be mentioned that a restriction method can be formulated in terms of not changing the set $\mathcal{H}$ but to implicitely making it compact by adding a term in the objective with certain compactness properties, something that is dealt with in section 6.

## 3 NUMERICAL TEST PROBLEMS

Four numerical test problems are chosen to illustrate and validate the different restriction methods. Each of the Figures 2-5 shows a structural domain in which an optimal density is to be distributed. The parts of the boundary where the displacements are fixed are indicated by gray and the applied forces are indicated by arrows. For the compliant mechanisms, Figures 4 and 5, the parts of the boundary that are in contact with a workpiece are indicated by a black patch that is connected to a spring. The thin arrows in these figures show the direction in which the maximized force should act. The material for each of the test problems is isotropic with a Young's modulus of 1000.0 and a Poisson's ratio of 0.29.

### 3.1 Maximum Stiffness Problems

The problems that are considered for stiffness maximization, or compliance minimization, are two classical benchmark problems in topology optimization.

The first one is a cantilever beam shown in Figure 2. The dimensions of the structural domain are $3.2 \times 2.0$ and the optimal structure should occupy no more than 50% of this domain. The structure is fixed along the left vertical edge and a vertical line load is applied at the center of the right vertical egde. The magnitude of the line load integrated is 1.0. Symmetry allows for performing the computations on the upper half of the domain.

The second problem is an MBB beam shown in Figure 3. The dimensions are $6.0 \times 1.0$ and, again, the amount of material is limited to 50% of the structural domain. Here the displacements are fixed in the vertical direction at the bottom corners as indicated in the figure. The singularity of the stiffness matrix is eliminated by considering only the left half of the domain for computations along with appropriate symmetry conditions. A vertical line load is applied at the top center of the domain with a magnitude of 1.0 integrated.

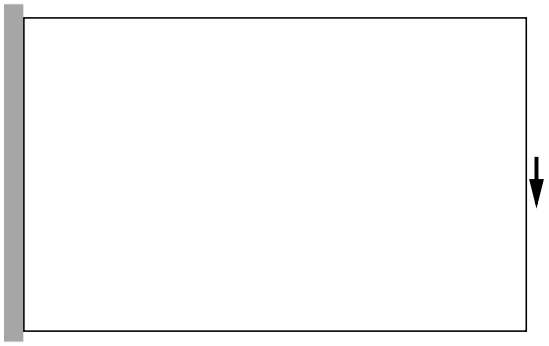

**Figure 2.** A cantilever beam

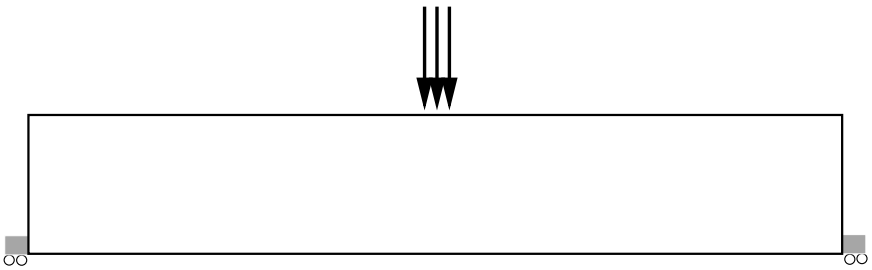

**Figure 3.** An MBB beam

### 3.2 Compliant Mechanism Problems

The two problems for designing compliant mechanisms have previously been treated in for instance [23].

The first problem is a force inverter mechanism shown in Figure 4. The structural domain is a square of dimensions $2.0 \times 2.0$ with forces and fixed displacements prescribed on the left vertical edge. The applied force is converted into a force in the opposite direction on the center of the right vertical edge. The magnitude of the applied force integrated is 1.0 and similarily, the magnitude of the stiffness of the workpiece integrated is 1000.0. The compliance is not allowed to exceed 0.1, which corresponds to an average input displacement of approximately 0.1. The maximum amount of material allowed is 20% of the domain and the computations are performed on the upper half.

The last problem is a gripper mechanism shown in Figure 5. The dimensions of the structural domain are again $2.0 \times 2.0$ but with a patch of dimensions $0.5 \times 0.5$ removed from the right center side of the square to form a gap. As for the force inverter mechanism, forces and fixed displacements are prescribed on the left vertical edge. This applied force should result in a force on a workpiece situated in the gap as shown in the figure. The magnitude of the applied force integrated is 1.0 and the magnitude of the stiffness of the workpiece integrated is 500.0 on each of the two considered parts of the boundary. The compliance is not allowed to exceed 0.1, which again corresponds to an average input displacement of 0.1. The maximum amount of material allowed is 20% of the domain and only the upper half is subject for computations. Because of the current implementation, the state problem is solved with the upper half of the gap included as well, in which the density is kept constant, $\rho = \rho_\epsilon$.

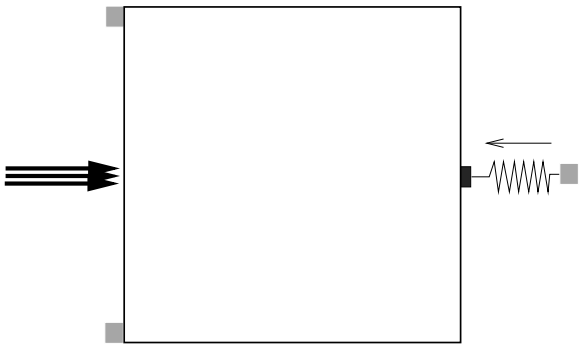

**Figure 4.** A force inverter mechanism

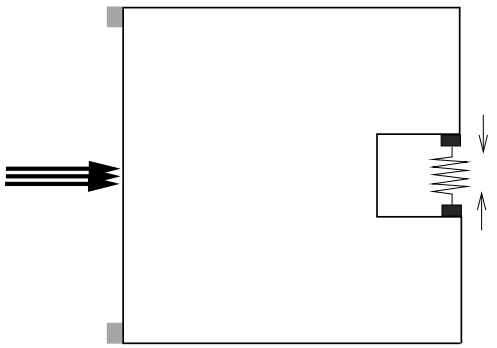

**Figure 5.** A gripper mec hanism

## 4 NUMERICS

### 4.1 The Discrete State Problem

Following a standard finite element procedure, the structural domain of each of the numerical examples in the previous section is discretized in to a uniform mesh of $N^h$ four noded bilinear finite elemen ts. The densit y $\boldsymbol{\rho}$ is approximated elementwise constan t and the displacemen ts $\boldsymbol{u}$ are approximated bilinear within and continuous across the edge of each finite elemen t. Let $\rho^h$ denote the discrete density, $\rho_i^h$ the value of the discrete density in element $i$ and $\boldsymbol{u}^h$ the vector of nodal values of the discrete displacemen ts. The discrete state problem related to (3) is the following system of linear equations

$$\boldsymbol{K}_{\rho,k}\boldsymbol{u}^h = \boldsymbol{f}. \tag{7}$$

Here $\boldsymbol{K}_{\rho,k}$ is the global stiffness matrix which is the sum of the con tributions from the stiffness of the structure and the w orkpiece respectively,

$$\boldsymbol{K}_{\rho,k} = \boldsymbol{K}_\rho + \boldsymbol{K}_k.$$

The standard stiffness matrix $\boldsymbol{K}_\rho$ is the sum of element stiffness matrices weighted by elemen t stiffness values,

$$\boldsymbol{K}_\rho = \sum_{i=1}^{N^h} f_q(\rho_i^h)\boldsymbol{K}_i,$$

and $\boldsymbol{K}_k$ is a diagonal matrix with positive diagonal values $|k_i^h|$ that are non-zero only at indices corresponding to places where the structure is assumed in contact with the w orkpiece,

$$\boldsymbol{K}_k = \mathrm{diag}\{|k_i^h|\}.$$

The v alues $k_i^h$ are the mean v alues of the function $\boldsymbol{k}$ along the edge of one finite elemen t calculated just as the elemen ts of the right hand side force vector $\boldsymbol{f}$.

It should be noted that a rigorous finite elemen t discretization of the integral (1) w ould not result in a diagonal stiffness matrix. The reason for approximating this matrix diagonal is due to computational simplicity and to the belief that this appro ximation is accurate enough to establish very similar n umerical results. The matrix $\boldsymbol{K}_k$ can be seen as a lumped approximation of the true stiffness matrix.

### 4.2 The Discrete Optimization Problems

Let $\boldsymbol{u}^h(\rho^h)$ be the solution to (7) corresponding to the discrete density $\rho^h$. The compliance $\tilde{\ell}$ and force on the workpiece $\tilde{t}_k$ now have the following discrete counterparts,

$$\begin{aligned} \tilde{\ell}^h(\rho^h) &= \boldsymbol{f}^T \boldsymbol{u}^h(\rho^h) \\ \tilde{t}_k^h(\rho^h) &= -\boldsymbol{k}^{hT} \boldsymbol{u}^h(\rho^h), \end{aligned} \tag{8}$$

where $\boldsymbol{k}^h$ is the vector with values $k_i^h$ described in the previous section. The discrete optimization problems corresponding to $(\boldsymbol{P})_{\text{stiff}}$ and $(\boldsymbol{P})_{\text{mech}}$ can be posed as

$$(\boldsymbol{P})^h_{\text{stiff}} \quad \begin{cases} \min\limits_{\rho^h} & \tilde{\ell}^h(\rho^h) \\ \text{s.t.} & \sum_{i=1}^{N^h} m_i^h \rho_i^h \le \overline{V} \\ & \rho_\epsilon \le \rho_i^h \le 1 \qquad i = 1, \dots, N^h \end{cases}$$

and

$$(\boldsymbol{P})^h_{\text{mech}} \quad \begin{cases} \min\limits_{\rho^h} & \tilde{t}_k^h(\rho^h) \\ \text{s.t.} & \sum_{i=1}^{N^h} m_i^h \rho_i^h \le \overline{V} \\ & \tilde{\ell}^h(\rho^h) \le \overline{\ell} \\ & \rho_\epsilon \le \rho_i^h \le 1 \qquad i = 1, \dots, N^h, \end{cases}$$

where $m_i^h$ is the measure of the $i$:th finite element.

### 4.3 Sensitivity Analysis

In order to solve the problems $(\boldsymbol{P})^h_{\text{stiff}}$ and $(\boldsymbol{P})^h_{\text{mech}}$ with standard optimization algorithms (at least of first order), sensitivities of the involved functions with respect to changes in the density $\rho^h$ are required. Since calculating the sensitivities of the volume constraint is straightforward, this section focusses on the two objective functions.

The sensitivities of the objective functions can be obtained by differentiating (7) and (8) which for the compliance yields

$$\frac{\partial \tilde{\ell}^h}{\partial \rho_j^h} = -f_q'(\rho_j^h) \boldsymbol{u}^{hT} \boldsymbol{K}_j \boldsymbol{u}^h.$$

A similar approach with the force on the workpiece yields

$$\frac{\partial \tilde{t}_k^h}{\partial \rho_j^h} = f_q'(\rho_j^h) \boldsymbol{\lambda}^{hT} \boldsymbol{K}_j \boldsymbol{u}^h,$$

where $\boldsymbol{\lambda}^h$ is the solution to the following adjoint equation

$$\boldsymbol{K}_{\rho,k} \boldsymbol{\lambda}^h = \boldsymbol{k}^h.$$

### 4.4 Numerical Algorithms and Strategies

The discrete problems in this section (together with extensions throughout the paper) are implemented mainly in C++ but with some aid of Fortran 77 to improve the computational efficiency. The optimization problems are solved with MMA (Method of Moving Asymptotes) [37], an optimization algorithm that is based on the idea of sequential convex approximations. In each iteration the system (7) is solved with an $LDL^T$-factorization of the stiffness matrix followed by a forward substitution, elimination of diagonal elements and a backward substitution which yields the sensitivities of the involved functions. Assuming that $\rho^h$ is the considered design variable †, an approximating separable subproblem is formed where each of the involved functions is on the following form

$$\sum_{i=1}^{N^h} \left\{ \frac{p_i}{\rho_i^h - l_i} - \frac{q_i}{u_i - \rho_i^h} \right\}.$$

The parameters $p_i$ and $q_i$ are chosen so that the sensitivities coincide with the ones that are obtained from the sensitivity analysis and so that the subproblem is convex. Because of the small number of constraints in $(\boldsymbol{P})^h_{\text{stiff}}$ and $(\boldsymbol{P})^h_{\text{mech}}$, the subproblem is solved with a dual method which in turn yields a design suggestion for the next iteration. The parameters $l_i$ and $u_i$ are the moving asymptotes that are continuously updated in order to control the optimization procedure. For details concerning the MMA, the reader may consult [37]. Other optimization algorithms used in this context include so called optimality criteria methods, see [1] and references therein, and sequential linear programming [20, 23, 38].

Regardless of the type of restriction, the problems $(\boldsymbol{P})^h_{\text{stiff}}$ and $(\boldsymbol{P})^h_{\text{mech}}$ are well known to be non-convex when some kind of penalization is introduced. Thus it may happen that an obtained numerical solution is only a local optimum to the considered problem. To prevent this from occurring, continuation strategies are often suggested. Continuation means that a sequence of problems is solved where the solution to each problem is used as a starting solution for the next. The sequence of problems are chosen so that the "degree" of non-convexity is gradually increased and hopefully the final solution is, if not a global optimum, at least better than a solution that is obtained without a continuation strategy. For the problems $(\boldsymbol{P})^h_{\text{stiff}}$ and $(\boldsymbol{P})^h_{\text{mech}}$ this could for instance mean that the parameter $q$ in the material interpolation function $f_q$ is gradually increased from $q = 1$ to some $q = \overline{q}$. In [39], by considering some small scale examples, it is shown that this strategy does not necessarily guarantee that a global optimum is reached. In this work, numerous types of continuation strategies were applied to the considered problems, for instance the one just mentioned. In most cases however, the solutions that are obtained in this way turn out to be worse than the ones that are obtained without any continuation. Based on this experience, all numerical examples in this paper are solved without a continuation strategy except in one particular case, see section 6.1.

In the numerical examples, the parameter $\rho_\epsilon$ always has the value that yields $f_q(\rho_\epsilon) \approx 10^{-9}$ for the chosen penalty parameter $q$ and the convergence criterion is given by the following. An optimal solution is considered to be reached when the difference in max-norm between two successive design suggestions is less than $10^{-4}$. The reason for choosing this strict criterion is that for compliant mechanisms, small changes in the design during a long time does in general result in a major change in the shape of the structure even

† In the problems $(\boldsymbol{P})_{\text{stiff}}$ and $(\boldsymbol{P})_{\text{mech}}$ there is no distinction between the design variable and the density $\rho$ since the optimization is with respect to this variable. In sections 5 and 7.2, a design variable will be introduced that is purely a mathematical help variable with no physical interpretation. The optimization will be with respect to this variable and the physical density $\rho$ will be determined by a design-to-density mapping.

though the objective function is only slightly improved. In appendix A, table 1 presents some computational data from the numerical examples in this paper. The examples are named $C_i, M_i, I_i$ and $G_i$ where the capital letter indicates what test problem is solved and the subindex $i$ refers to the order in which they appear in the text. In each of the upcoming figures, the figure text reveals what particular example is shown. As can be seen from table 1, the number of optimization iterations is in general very high due to the mentioned convergence criterion and in practice it would often suffice to perform a few hundred iterations to obtain a reasonable solution. This number may vary depending on the specific problem and type of restriction considered. In appendix B, three types of restriction methods for compliance minimization are compared from a more practical point of view.

## 5 FINITE DIMENSIONAL SET OF ADMISSIBLE DESIGNS

Any of the problems in section 4.2 is well-posed and hence it should not be troublesome to establish at least a locally optimal solution to this finite dimensional problem. However, unless the corresponding infinite dimensional problem is well-posed, it is likely that this solution would contain checkerboards [33, 40, 41] and/or structural parts that are no more than one or two elements wide, these being regions in the structural domain from which the structural responses are quite misleading. A refinement of the finite element mesh does in general not help as this would give a completely different design suggestion, probably with even more checkerboards and thin structural members [41]. As indicated in section 2.4, the fundamental problem is that there can be no connection between the finite dimensional optimization problem and any well-posed infinite dimensional problem. Another, perhaps more intuitive, way of putting it is that the discretizations of design and displacements are coupled, a refinement of the displacement mesh implies a refinement of the design mesh. For any discretization level, the discrete set of admissible displacements is incapable of giving accurate information of the state of all the admissible designs. This suggests that a refinement of the finite element mesh should be possible without refining the set of designs. The set of designs is made finite dimensional a priori and hence independent of the numerical discretization.

### 5.1 Problem Formulation

Referring to section 2.4, the restricted set $\tilde{\mathcal{H}}$ is chosen

$$\tilde{\mathcal{H}} = \{\rho \in L^\infty(\Omega) \quad | \quad \rho = \sum_{i=1}^{N^H} \xi_i \phi_i, \quad \int_\Omega \rho \leq V, \quad \rho_\epsilon \leq \xi_i \leq 1\}. \tag{9}$$

Here $N^H$ is a fixed number that is independent of the numerical discretization, $\xi_i$ are the components of the design vector $\boldsymbol{\xi} \in \boldsymbol{R}^{N^H}$ and $\phi_i$ are suitably chosen basis functions. These basis functions should be chosen first so that $\tilde{\mathcal{H}} \subset \mathcal{H}$ and second so that $\tilde{\mathcal{H}}$ allows for a rich supply of structures. The definition of $\tilde{\mathcal{H}}$ above is assumed for the problem $(\boldsymbol{P})_{\text{stiff}}$ and should of course be complemented with the compliance constraint when considering the problem $(\boldsymbol{P})_{\text{mech}}$. It should be noted that $\rho$ is not the design variable as the optimization is now with respect to the vector $\boldsymbol{\xi}$. The density $\rho$ is determined by the linear design-to-density mapping given in the definition of $\tilde{\mathcal{H}}$.

### 5.2 The Basis Functions

For the description of the basis functions that are used for the numerical examples, the rectangular structural domain is embedded in a uniform mesh with elements of size $H \times H$ so that it is aligned along the mesh and so that each corner point of the structural domain

coincide with some nodal point of the considered mesh. The basis functions are chosen as gaussian bells that are centered at the nodal points of this mesh. At node $i$ with coordinates $(x_i, y_i)$, the corresponding basis function $\phi_i$ is given by

$$\phi_i(x,y) = \frac{1}{\pi} e^{-\frac{(x-x_i)^2+(y-y_i)^2}{H^2}}.$$

For practical purposes, a neighbourhood of the point $(x_i, y_i)$ is chosen, outside of which the contribution from $\phi_i$ is put equal to zero. For the numerical examples, this neighbourhood is a quadrant of dimensions $6H \times 6H$ that is aligned along the mesh and centered at $(x_i, y_i)$. The $N^H$ basis functions that are considered for computations are those that can give a non-zero contribution to the density $\rho$, namely those that are situated sufficiently close to the structural domain. It should be mentioned that with this choice of basis functions, $\tilde{\mathcal{H}}$ is not completely contained in $\mathcal{H}$ because the constraint $\rho_\epsilon \leq \xi_i \leq 1$, $i = 1, ..., N^H$ does not imply $\rho_\epsilon \leq \rho \leq 1$ a.e. in $\Omega$. However, it is almost valid in the sense that the deviation from the last constraint is only a fraction of a percent. This set of basis functions has previously been used in the theory of approximate approximations [42], a numerical solution method for partial differential equations.

### 5.3 Numerics and Sensitivity Analysis

When solving the problem numerically, one would have to determine the discrete density $\rho^h$ that is to be used for solving the state problem (7). The element values of $\rho^h$ are in this implementation determined by the sample values of $\rho$ in the centroids of the finite elements,

$$\rho_j^h = \sum_{i=1}^{N^H} \xi_i \phi_{ij},$$

where $\phi_{ij}$ is the value of $\phi_i$ at the centroid of element $j$. It remains to determine the sensitivities of the involved functions with respect to the design variable $\boldsymbol{\xi}$. By the chain rule in differential calculus, it is only necessary to determine the sensitivities of $\rho^h$ with respect to $\boldsymbol{\xi}$ and combine them with the sensitivities in section 4.3. These are given by

$$\frac{\partial \rho_j^h}{\partial \xi_i} = \phi_{ij}.$$

### 5.4 Numerical Results

The first numerical example is the cantilever beam which is solved with $H = 0.1$ for three different displacement meshes. The material interpolation function is given by (5) with $q = 6$ and the solutions are shown in Figure 6. As illustrated in this figure, the boundary description of an optimal structure is blurry and the few number of design variables in general makes the structural parts rather jagged despite a fine displacement mesh. On the other hand, the few number of design variables allows for a fast optimization procedure in comparison to the other methods that are presented in this paper, cf. table 1. Worth mentioning is also that the number of optimization iterations is virtually independent of the displacement mesh as it should be since the number of design variables does not change when the displacement mesh is refined.

The second numerical example is the inverter mechanism which is solved for $H = 1/30$ and $H = 1/15$ with the respective solutions shown in Figure 7. The same material interpolation function as for the previous example is used. Noticable is that structural members that are aligned along and diagonal to the mesh are in fact straigh t and smooth, which is significant for the chosen set of basis functions. The reason for obtaining the weakly gray density

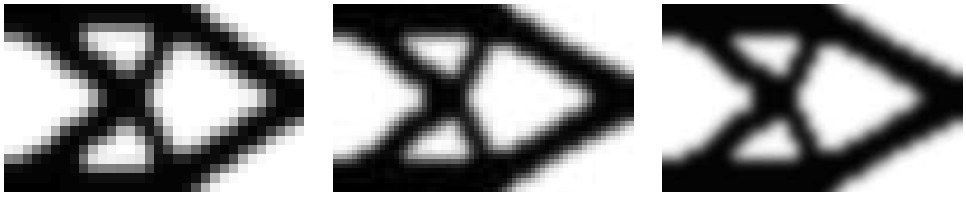

**Figure 6.** The cantilever beam ($C_1 - C_3$) with a finite dimensional set of designs

region appearing in the solution $I_2$ is believed to be partly because of the few number of design variables. There is no way of eliminating the gray without violating the compliance constraint for this choice of $H$. In the solution $I_1$, which is solved with approximately four times as many design variables, the gray is eliminated by at the same time slightly changing the shape of the structure. These solutions should be compared to the inverter mechanisms in section 7.2.2.

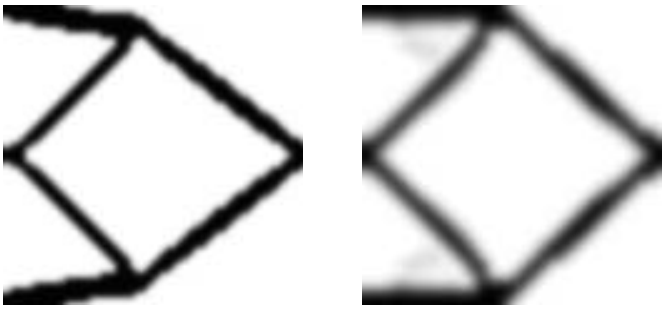

**Figure 7.** The inverter mechanism ($I_1 - I_2$) with a finite dimensional set of designs

## 6 BOUNDS ON THE DESIGN GRADIENT

A minimizing sequence of either one of the problems in section 2.2 is in general characterized by increasingly oscillating designs. A way to measure oscillations of a function is through some norm on the distributional gradient, hence it would be natural to impose a bound on such a norm. Straightforward choices of norms would be the common $L^p$ norms, i.e. impose

$$\|\nabla\rho\|_p \leq C_p < \infty, \quad 1 \leq p \leq \infty, \tag{10}$$

or add a term in the objective on the form

$$c_p\|\nabla\rho\|_p \quad 1 \leq p \leq \infty, \tag{11}$$

with $c_p > 0$. In the former case, the restricted set $\tilde{\mathcal{H}}$ in section 2.4 is exactly the set $\mathcal{H}$ with the additional constraint (10). In the latter case, the set $\mathcal{H}$ is not explicitely changed, but the measure (11) implies that the optimal solution satisfies (10) for some $C_p$.

Since $\nabla\rho$ may not exist as a function, it is at this moment not clear what $\|\nabla\rho\|_p$ means. The following definition is taken,

$$\|\nabla\rho\|_p := \sup\{\int_\Omega \rho \ \mathrm{div}\boldsymbol{\phi} \quad | \quad \boldsymbol{\phi} \in \boldsymbol{C}_0^\infty(\Omega), \quad \|\boldsymbol{\phi}\|_q \leq 1\}, \tag{12}$$

where $q$ is the conjugate exponent of $p$. A constraint of type (10) or a measure of type (11) implies that for a minimizing sequence $\rho$, $\|\nabla\rho\|_p$ is uniformly bounded and existence of solutions follows, loosely speaking, from lower semi-continuity of $\|\cdot\|_p$ and the Rellich-Kondrachovs compactness theorem [26]. For $1 < p \leq \infty$, this means that $\rho$ belongs to the Sobolev space $W^{1,p}(\Omega)$ and $\|\cdot\|_p$ is the usual $\boldsymbol{L}^p$ norm. For $p = 1$ however, $\rho$ belongs to a superspace of $W^{1,1}(\Omega)$ denoted $BV(\Omega)$, functions of bounded variation, which plays an important role in e.g. the theory of plasticity [43] and minimal surfaces [44]. When $p = \infty$, the gradient is bounded pointwise which is the strongest constraint. The three cases $p = 1$, $1 < p < \infty$ and $p = \infty$ will be treated separately in the following three subsections.

### 6.1 Perimeter Constraint

For $p = 1$, (12) is the total variation of $\rho$. When $\rho$ is the characteristic function of a set, the total variation is called the perimeter of the set. For a set $\omega \subset \Omega$ with sufficiently smooth boundary, it can be shown that

$$\|\nabla\chi_\omega\|_1 = |\partial\omega \cap \Omega|. \tag{13}$$

In other words, the perimeter of $\omega$ is equal to the measure of the part of $\partial\omega$ that is contained in $\Omega$. Since this suggests that structural parts of the optimal structure are preferrably situated at the boundary of $\Omega$, this total variation is replaced by

$$TV(\rho) = \sup\{\int_{\boldsymbol{R}^2} \rho \,\mathrm{div}\boldsymbol{\phi} \quad | \quad \boldsymbol{\phi} \in \boldsymbol{C}_0^\infty(\boldsymbol{R}^2), \quad |\boldsymbol{\phi}| \leq 1 \text{ almost everywhere}\},$$

where $\rho$ is assumed extended by zero outside $\Omega$. This does not change any of the theoretical results mentioned above, and for $\omega \subset \Omega$ with sufficiently smooth boundary, cf. (13),

$$TV(\chi_\omega) = |\partial\omega|.$$

The difference is that this variation takes into account the variation over the boundary of $\Omega$.

For a problem very similar to the considered problem, existence of solutions was shown by Ambrosio and Butazzo [45] and in the context of topology optimization, the problem was later treated theoretically by Petersson [46]. A numerical treatment was first provided by Haber *et al.* [47] and has since been followed up by for instance Duysinx [48] and Beckers [49]. In Beckers [49] the problem is solved with discrete constraints and it also includes topology optimization of 3-dimensional structures. Perimeter constrained topology optimization in 3 dimensions has also been treated by Fernandez *et al.* [50].

#### *6.1.1 Numerics*

The numerical approximation of the perimeter, or total variation, is something that has drawn attention. For this exposition, it is for simplicity assumed that a 2-dimensional rectangular structural domain is discretized uniformly so that $h$ denotes the length and width of each finite element and $n_x$ and $n_y$ denote the number of finite elements in each coordinate direction. Each element is given an index $(i,j)$, $i = 1,...,n_x$, $j = 1,...,n_y$ that indicates the position of the element in the finite element mesh in an obvious way. Furthermore, let $\rho^h_{i,j}$ be the density value of $\rho^h$ that corresponds to element $(i,j)$ and for any $i \leq 0$, $j \leq 0$, $i > n_x$ or $j > n_y$, $\rho^h_{i,j} = 0$. To keep the formulas in this section of reasonable length, let

$$\delta^{\rightarrow}_{i,j} = |\rho^h_{i+1,j} - \rho^h_{i,j}|, \qquad \delta^{\uparrow}_{i,j} = |\rho^h_{i,j+1} - \rho^h_{i,j}|,$$

$$\delta^{\nearrow}_{i,j} = |\rho^h_{i+1,j+1} - \rho^h_{i,j}|, \qquad \delta^{\nwarrow}_{i,j} = |\rho^h_{i,j+1} - \rho^h_{i+1,j}|.$$

A straightforward evaluation of the total variation of an elementwise constant density $\rho^h$ yields

$$TV_2(\rho^h) = h\left\{\sum_{i=0}^{n_x}\sum_{j=1}^{n_y}\delta_{i,j}^{\rightarrow} + \sum_{i=1}^{n_x}\sum_{j=0}^{n_y}\delta_{i,j}^{\uparrow}\right\}. \tag{14}$$

This approximation takes differences of density values in the 2 coordinate directions which explains the introduction of the subindex. It is well known that using this formula will favour a structure with a large portion of its boundary aligned along the cartesian coordinate axes [46, 47]. In fact, even for a smooth function $\rho$ that is appropriately approximated as elementwise constant $\rho^h$, this formula will not converge to the correct total variation which is unfortunate. Considering that for a smooth function $\rho$,

$$TV(\rho) = \int_{\boldsymbol{R}^2} |\nabla\rho|,$$

an alternative to (14) would be to make a finite difference approximation of the gradient of $\rho$ (neglecting the fact that it may not be differentiable) and then perform numerical integration. One way of doing this yields the following approximation of the total variation,

$$\tilde{TV}_2(\rho^h) = \frac{h}{\sqrt{2}}\sum_{i=0}^{n_x}\sum_{j=0}^{n_y}\sqrt{\delta_{i,j}^{\rightarrow 2} + \delta_{i,j+1}^{\rightarrow 2} + \delta_{i,j}^{\uparrow 2} + \delta_{i+1,j}^{\uparrow 2}}. \tag{15}$$

It is straightforward, although tedious, to verify that for a smooth function $\rho$ that is appropriately approximated as elementwise constant $\rho^h$, this formula will in fact converge to the correct total variation,

$$\tilde{TV}_2(\rho^h) \to TV(\rho), \quad h \to 0.$$

This is illustrated in the first graph of Figure 8, which shows the deviation from the true total variation of a rotating plane for some numerical approximations. The horizontal solid line at $y = 0$ corresponds to $\tilde{TV}_2$ and the dashed line corresponds to $TV_2$. However, for a non-smooth function, the deviation of the two approximations appears similar which is illustrated in the second graph of Figure 8. This graph shows the deviation from the true total variation of a rotating edge for some numerical approximations and the dashed line corresponds to both $\tilde{TV}_2$ and $TV_2$. It is seen that the deviation can be as large as $\approx 41\%$ but this can be significantly reduced by considering differences of density values in 4 directions, namely horizontally, vertically and also diagonally in the finite element mesh. This is done in [51] and the suggested approximation is

$$\begin{aligned} TV_4(\rho^h) = \quad & (\sqrt{2}-1)h\left\{\textstyle\sum_{i=0}^{n_x}\sum_{j=1}^{n_y}\delta_{i,j}^{\rightarrow} + \sum_{i=1}^{n_x}\sum_{j=0}^{n_y}\delta_{i,j}^{\uparrow}\right\} + \\ & \tfrac{\sqrt{2}-1}{\sqrt{2}}h\left\{\textstyle\sum_{i=0}^{n_x}\sum_{j=0}^{n_y}\delta_{i,j}^{\nwarrow} + \sum_{i=0}^{n_x}\sum_{j=0}^{n_y}\delta_{i,j}^{\nearrow}\right\}. \end{aligned}$$

This reduces the anisotropy to $\approx 8\%$, see the dash-dotted line in both graphs in Figure 8. An attempt to improve on this is here made through the following ansatz,

$$\begin{aligned} \tilde{TV}_4(\rho^h) = \quad & \alpha\tfrac{h}{\sqrt{2}}\textstyle\sum_{i=0}^{n_x}\sum_{j=0}^{n_y}\sqrt{\delta_{i,j}^{\rightarrow 2} + \delta_{i,j+1}^{\rightarrow 2} + \delta_{i,j}^{\uparrow 2} + \delta_{i+1,j}^{\uparrow 2}} + \\ & \beta\tfrac{h}{2}\textstyle\sum_{i=0}^{n_x+1}\sum_{j=0}^{n_y+1}\sqrt{\delta_{i,j-1}^{\nearrow 2} + \delta_{i-1,j}^{\nearrow 2} + \delta_{i-1,j-1}^{\nwarrow 2} + \delta_{i,j}^{\nwarrow 2}}. \end{aligned}$$

Sufficient for

$$\tilde{TV}_4(\rho^h) \to TV(\rho), \quad h \to 0$$

to hold when $\rho$ is smooth is to require $\alpha + \beta = 1$. Unfortunately, the lowest anisotropy for a rotating edge given this condition is $\approx 31\%$ for $\alpha = \beta = 0.5$, which is illustrated by the solid line in the second graph of Figure 8. For $\alpha = \beta = \sqrt{2} - 1$, the anisotropy for $\tilde{TV}_4$ coincide with $TV_4$ which however makes the variation for a rotating plane underestimated by $\approx 17\%$.

The sensitivity analysis of the expression for $\tilde{TV}_4$ with respect to $\rho^h$ is straightforward but rather lengthy and is therefore omitted.

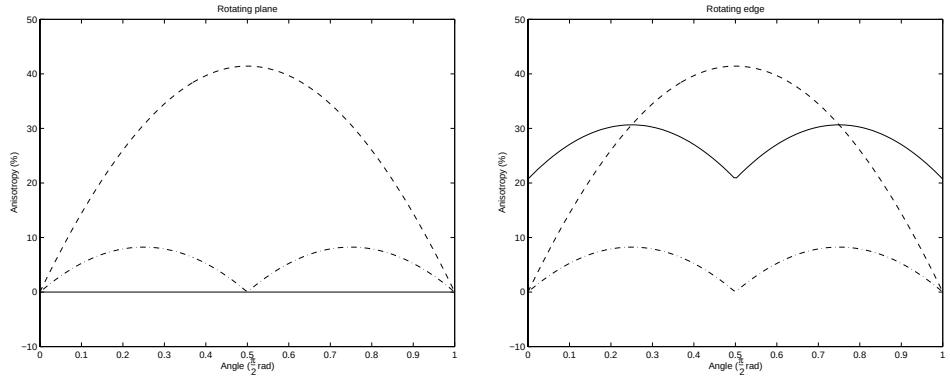


**Figure 8.** Anisotropies for the different perimeter approximations

### *6.1.2 Numerical results*

Two numerical examples are presented where a variation term is added in the objective as in (11). The reason for not imposing a constraint on the form (10) is because the former approach has shown to be more stable numerically. First, the cantilever beam is solved with the $TV_4$ approximation for two different values of $c_1$. The two solutions are shown in Figure 9 and the $TV_4$ values are 25.6 and 19.6 obtained with the $c_1$ values $2.5 \cdot 10^{-5}$ and $1.5 \cdot 10^{-4}$ respectively. The material interpolation function is chosen as (5) with $q = 2.5$ and $q = 6$ respectively. It is immediately noted that the boundary description is very sharp in comparison to for instance the solutions in Figure 6. This is expected since intermediate density values are suppressed and $\rho$ is certainly allowed to be non-smooth. This can also be seen in Figure 10, which shows the gripper mechanism solved for three different meshes with the $\tilde{TV}_4$ approximation, $\alpha = \beta = 0.5$. The same material interpolation function is used but this solution requires that $q$ is gradually increased. A continuation strategy is used where 200 iterations are performed for $q = 2$ and $q = 3.5$ before the final solution is obtained for $q = 6$. The $\tilde{TV}_4$ values for these three structures are 28.2, 29.4 and 30.2 for a $c_1$ value of $8.3 \cdot 10^{-3}$.

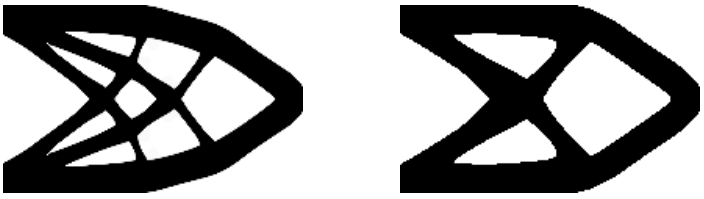

**Figure 9.** The cantilever beam ($C_4 - C_5$) with a $TV_4$ constraint

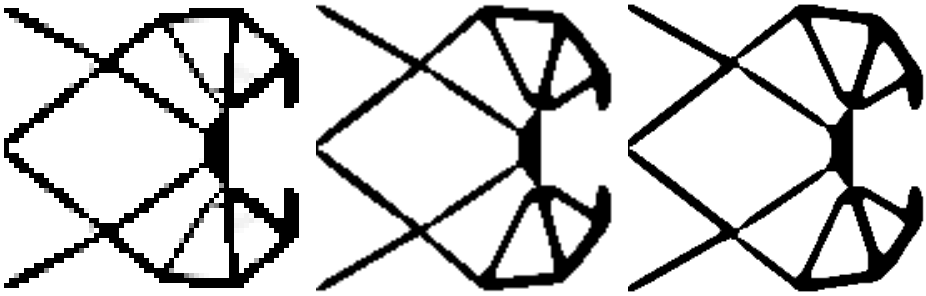

**Figure 10.** The gripper mechanism ($G_1 - G_3$) with a $\tilde{TV}_4$ constraint

Regardless of the particular choice of perimeter approximation, the solution procedure for the optimization problem with a perimeter constraint is rather unstable and sensitive to local optima. The experience is that it requires delicate parameter adjustments for each individual problem. The solutions presented here are obtained through many trials and errors and it is hard to guarantee that the solutions that are presented here are true global optima for the chosen parameters. In fact, it will be apparent that the solution $C_5$ in Figure 9 is only a local optimum when consulting section 7.3.2. It should be noted that the perimeter problem appears to has been solved more successfully by others, see for instance [48, 49], but with a solution algorithm especially tailored for this problem. In these references, some heuristically estimated second order information for the perimeter function is used to stabilize the numerical procedure. Inspired by this and the fact that $\tilde{TV}_4$ is sometimes smooth (in comparison to $TV_4$ which never is), the author tried to improve the solution procedure but unsuccessfully. Another disadvantage is of course that the value of $\bar{c}_1$ (or $C_1$) can in practice only be determined by experiments. All this makes it hard to give a general description on how to solve these kinds of problems and perimeter constrained topology optimization is not recommended in practice.

## 6.2 $L^p$-constraint

The case $1 < p < \infty$ is now considered. A numerical treatment of this problem in the context of topology optimization has never appeared in the literature although something similar has been suggested as an alternative to the perimeter constraint. In Bendsøe [1] for instance, a slightly modified problem is proved to be well-posed when $p = 2$ and the same result was obtained by Bendsøe [52] in the context of optimization of solid, elastic plates.

### *6.2.1 Numerics and sensitivity analysis*

The assumptions and notation from section 6.1.1 are kept. The numerical approximation for $\|\nabla\rho\|_p$ is denoted $D_p(\rho^h)$ and is chosen as

$$D_p(\rho^h) = \frac{h^{\frac{2-p}{p}}}{\sqrt{2}} \left\{ \sum_{i=1}^{n_x-1} \sum_{j=1}^{n_y-1} \left\{ \delta_{i,j}^{\rightarrow 2} + \delta_{i,j+1}^{\rightarrow 2} + \delta_{i,j}^{\uparrow 2} + \delta_{i+1,j}^{\uparrow 2} \right\}^{\frac{p}{2}} \right\}^{\frac{1}{p}}, \tag{16}$$

again based on finite differences and numerical integration. Referring to (15), it is interesting to note that $D_1 = \tilde{TV}_2$ with the exception of now not considering elements outside the structural domain.

The sensitivity analysis for a general $p$ is just as lengthy as for $\tilde{TV}_4$ and only the case $p = 2$ is studied. To avoid taking the square-root into account, the sensitivities for $D_2(\rho^h)^2$

are considered. For an element $(i,j)$ in the interior of the structural domain it holds that

$$\frac{\partial}{\partial \rho^h_{i,j}} D_2(\rho^h)^2 = 8\rho^h_{i,j} - 2\rho^h_{i-1,j} - 2\rho^h_{i,j-1} - 2\rho^h_{i+1,j} - 2\rho^h_{i,j+1}$$
$$\frac{\partial^2}{\partial \rho^{h2}_{i,j}} D_2(\rho^h)^2 = 8.$$

Notewor thy is that $D_p^p$ is smooth for every even $p$ as opposed to any perimeter approximation.

### *6.2.2 Numerical results*

Just as for the perimeter, a term in the objective is added for numerical purposes. The values $p = 2, 4, 8$ are chosen and the norm in (11) is raised to these powers to simplify the sensitivity analysis, i.e. for each individual $p$ the following term is added in the objective

$$\tilde{c}_p D_p(\rho_h)^p.$$

The first example is the MBB beam which is solved for $p = 2$ and two different values of $\tilde{c}_2$. The material interpolation function is given by (5) with $q = 2.5$ and $q = 6$ respectively and the solutions are shown at the top in Figure 11. The values of $D_2$ for the two solutions are 49.5 and 20.0 for $\tilde{c}_2$ values of $1.8 \cdot 10^{-6}$ and $5.6 \cdot 10^{-5}$. The same problem is solved for $p = 4$ and $p = 8$ with the corresponding solutions shown at the bottom in Figure 11. The material interpolation function is the same with $q = 6$ and the values of $D_4$ and $D_8$ for the two respective solutions are 15.9 and 11.4 for $\tilde{c}_4 = 8.3 \cdot 10^{-7}$ and $\tilde{c}_8 = 2.2 \cdot 10^{-9}$. From this it is seen that the amount of gray is increasing with increasing $p$ which suggests that these problems can be viewed as interpolations, in some vague sense, between perimeter and slope constrained topology optimization (see section 6.3). To strengthen this, it is interesting to estimate the constribution to $\|\nabla\rho\|_p$ from a structural bar with a width of $b$ and a length of $L$. Assuming that the bar occupies the domain

$$\Omega_{\text{bar}} = \{(x,y) \in \boldsymbol{R}^2 \quad | \quad -L/2 \le x \le L/2, \quad -b/2 \le y \le b/2\}$$

and that $\rho$ is there given by

$$\rho(x,y) = 1 - 2|y|/b,$$

this contribution is equal to

$$\Big(\int_{\Omega_{\text{bar}}} |\nabla\rho|^p\Big)^{\frac{1}{p}} = 2\frac{L^{\frac{1}{p}}}{b^{\frac{p-1}{p}}}. \tag{17}$$

As is expected, for $p = 1$ the length of the bar is measured and for $p = \infty$ the slope of the function $\rho$ is measured. In between, a combination of both length and slope is measured in the sense given by the formula.

Regarding the $\boldsymbol{L}^p$-constraint for a large $p$, the added term in the objective is in a sense ill-conditioned and there can be problems with convergence. For instance, the example $M_4$ with $p = 8$ above is solved with conservative asymptote updates in the MMA in order to converge properly, see [37]. Considering implementation aspects and numerical stability a suitable choice of $p$ would be $p = 2$. This also makes the function $D_2^2$ a quadratic function which can be taken advantage of. The problems above are solved with MMA but with the function $D_p^p$ approximated as quadratic and separable in each iteration which appears to somewhat stabilize the solution procedure.

The second example is the gripper mechanism with $p = 2$ and the same material interpolation function with $q = 6$. The problem is solved for three different meshes and the three solutions are shown in Figure 12. The $D_2$ values for these three structures are 25.0,

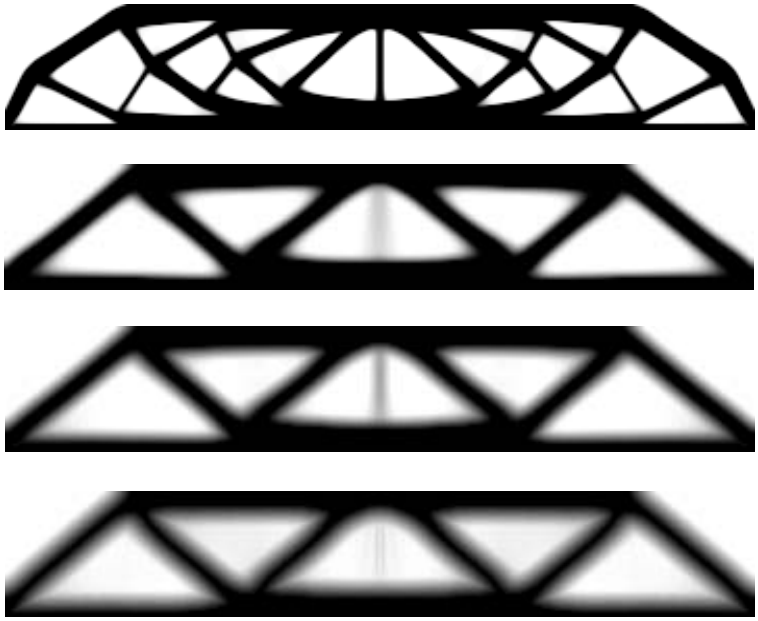

**Figure 11.** The MBB beam ($M_1 - M_4$) with an $\boldsymbol{L}^p$-constraint, $p = 2, 4, 8$

27.7 and 28.0 for a $\tilde{c}_2$ value of $1.0 \cdot 10^{-3}$. The stability of the solution procedure is very much improved compared to a perimeter constraint even when no second order information is used. Considering the three solutions in Figure 12, one can see that any non-smoothness of the numerical solution vanishes as the mesh is refined which reflects the fact that the true solution is smooth. That this effect is expected can also be seen from the numerical approximation (16) with $p = 2$ as a discontinuity in the design will contribute infinitely much as the mesh is infinitely refined. To obtain a smooth solution, it seems that a fine mesh is required in the lumped compliance regions which suggests that this restriction method should be combined with some kind of finite element adaptivity scheme similar to the one in [16, 30]. Despite all the advantages compared to using a perimeter constraint, the method can for the design of compliant mechanisms be extra sensitive to local optima. In addition to this, a main disadvantage is that there is no more straightforward way of determining the parameter $\tilde{c}_2$ than through trial and error.

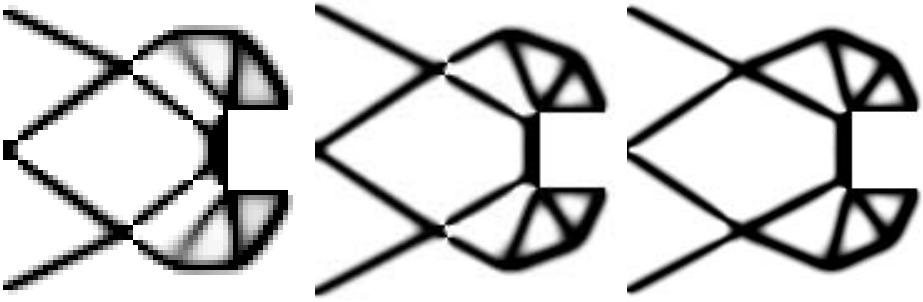

**Figure 12.** The gripper mechanism ($G_4 - G_6$) with an $\boldsymbol{L}^2$-constraint

### 6.3 Slope Constraint

As both the perimeter constraint and the $\boldsymbol{L}^p$-constraint are global constraints there is a problem regarding the choice of $c_p$ or $C_p$ depending on the choice of approach. More attractive from that point of view is to consider a pointwise constraint on the derivative of $\rho$, a slope constraint. In structural optimization this was introduced in the optimal design of elastic plates by Niordson [53] and a similar problem has been treated theoretically in optimal control by Hlaváček *et al.* [54]. Slope constraints in the context of topology optimization was introduced and treated by Petersson and Sigmund [38] although that paper considers a bound on the partial derivatives. Existence of solutions for that case is shown and the problem has also been treated later by Zhou *et al.* [55] which includes 3-dimensional topology optimization.

For slope constrained topology optimization, there is a simple relationship between a desired minimum width of the structural members $b_{\min}$ and the parameter $C_\infty$, namely (cf. (17) with $p = \infty$)

$$C_\infty \approx \frac{2}{b_{\min}}. \tag{18}$$

However, a bound on the slope of the density is from a numerical aspect not attractive since it results in many constraints, approximately 2 for each finite element. In [38], this is reported to be a significant drawback with the method. An algorithm for this problem that exploits the characteristics of the constraints is dealt with in [55] where it is reported that the incorporation of these constraints requires almost no extra computational cost. Since the optimization algorithm that is used in this paper is based on the assumption of a small number of constraints, this problem is not treated numerically here. From the discussion in the previous section however, it is believed that results very similar to ones obtained with a slope constraint can be obtained with an $\boldsymbol{L}^p$-constraint for a large $p$. It is for instance interesting to compare the MBB beam solution for $p = 8$ in Figure 11 with a corresponding solution with a slope constraint in [38]. Since a large $p$ in the former case could result in numerical problems and the physical interpretation of $\|\nabla\rho\|_p$ is not straightforward, an alternative would be to consider filters in topology optimization.

## 7 FILTERS

In image processing, a well known technique to reduce high frequency components in an image is through low pass filtering. As mentioned earlier, a minimizing sequence of designs to any of the problems $(\boldsymbol{P})_{\text{stiff}}$ and $(\boldsymbol{P})_{\text{mech}}$ contains many high frequency components which indicates that filters in some way could be useful in the context of topology optimization. In the literature, there have appeared at least three different suggestions on how to use filters appropriately in order to obtain a well behaved solution procedure. Two of these approaches are based on a mathematically well-founded problem formulation while one of them is not. Nevertheless, that is the first work on filters in topology optimization and gives an indication of the use of image processing techniques in this field.

### 7.1 Filtering the Sensitivities

A filter approach was first introduced by Sigmund [56] who uses it as a stabilizing measure in the numerical procedure. The idea is to use filtered sensitivities for the objective function in order to prevent too thin structural parts to appear in the optimal design. Since the measures taken are purely numerical, the expressions given in this section are referring to a modification of the problems $(\boldsymbol{P})^h_{\text{stiff}}$ and $(\boldsymbol{P})^h_{\text{mech}}$. With the same notation as previously and $\phi^h_{ij}$, $i = 1, \ldots, N^h$, $j = 1, \ldots, N^h$, denoting the considered filter components, the

sensitivities of the objective function $c$ to either one of the considered problems are filtered in the following way,

$$\frac{\tilde{\partial} c}{\partial \rho_i^h} = \frac{1}{\rho_i^h} \sum_{j=1}^{N^h} \rho_j^h \phi_{ij}^h \frac{\partial c}{\partial \rho_j^h}. \tag{19}$$

The filter components are for instance chosen as

$$\phi_{ij}^h = c_i \max(0, 1 - \frac{\text{dist}(e_i, e_j)}{R}), \tag{20}$$

where $c_i$ is a constant such that

$$\sum_{j=1}^{N^h} \phi_{\cdot j}^h = 1.$$

Here $e_i$ denotes the $i$:th finite element and $R$ is the filter radius that is intended to determine the minimum width of the structural parts. In the problem $(\boldsymbol{P})_{\text{mech}}^h$, the constraint on the compliance is filtered in exactly the same way. Although there is no theoretical justification for this method at the moment, the numerical experience has proved that it is quite effective. Moreover, the solutions have shown to be mesh independent, see [56], and it appears likely that there is some problem in infinite dimension that is in some sense connected to this algorithm. A numerical solution of the MBB beam with this technique is shown in Figure 13 with $R = 0.1$ and $q = 3$ in (4). Worth mentioning is that this approach has not been used only for compliance minimization [56] and design of compliant mechanisms [23] but also for e.g. multi-physics problems [57] and eigenvalue maximization [58].

**Figure 13.** The MBB beam ($M_5$) with filtered sensitivities

Something that is noted from experimenting with this algorithm is that it is very unstable when $\rho_\epsilon$ is small. The reason for this is that the filtered sensitivities in (19) can be of the order $1/\rho_\epsilon$ even when the true sensitivities are quite moderate. This can be cured by changing (19) to

$$\frac{\tilde{\partial} c}{\partial \rho_i^h} = \frac{1}{\sum_{j=1}^{N^h} \rho_j^h \phi_{ij}^h} \sum_{j=1}^{N^h} \rho_j^h \phi_{ij}^h \frac{\partial c}{\partial \rho_j^h},$$

which makes the modified sensitivities convex combinations of the true sensitivities. This also has a remarkable effect on the solutions as they become considerably more discrete valued. The first impression is however that the boundary description may sometimes be rather poor and the stability of the numerical procedure is worsened. The inverter mechanism is solved for $R = 0.1$ and $q = 6$ in (5) with this method and the solution is shown in Figure 14.

### 7.2 Filtering the Design

In Bruns and Tortorelli [25] the filter is introduced as a part of the problem formulation very similarily to the exposition in this section. The restricted set $\tilde{\mathcal{H}}$ is the following

$$\tilde{\mathcal{H}} = \{\rho \in \mathcal{H} \quad | \quad \rho = \int_{\boldsymbol{R}^2} \xi(\boldsymbol{y}) \phi(\cdot, \boldsymbol{y}) d\boldsymbol{y} \text{ for some } \xi \in L^\infty(\boldsymbol{R}^2, [\rho_\epsilon, 1])\}, \tag{21}$$

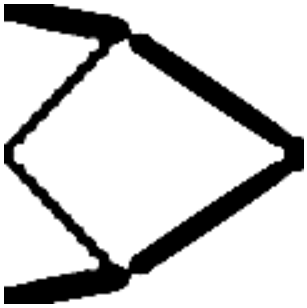

**Figure 14.** The inverter mechanism ($I_3$) with filtered sensitivities

where $L^\infty(\boldsymbol{R}^2, [\rho_\epsilon, 1])$ is the set of functions $\xi \in L^\infty(\boldsymbol{R}^d)$ that fulfil $\rho_\epsilon \leq \xi \leq 1$ almost everywhere. The integral kernel $\phi$ is a continuous variant of the filter that is proposed in the previous section, namely

$$\phi(\boldsymbol{x}, \boldsymbol{y}) = \frac{3}{\pi R^2} \max(0, 1 - \frac{|\boldsymbol{x} - \boldsymbol{y}|}{R}). \tag{22}$$

Proof of existence of solutions to a very similar problem formulation is given by Bourdin [59] where also numerical examples are presented that show the influence of the filter radius. Similarily to the approach with a finite dimensional set of admissible designs, see section 5, $\xi$ is the design variable and the density $\rho$ is determined through the compact design-to-density mapping given in the description of $\tilde{\mathcal{H}}$. Noticable is that this mapping assures that the slope is uniformly bounded,

$$\rho \in \tilde{\mathcal{H}} \quad \Rightarrow \quad \|\nabla \rho\|_\infty \leq \frac{3}{\pi R}, \tag{23}$$

so the set $\tilde{\mathcal{H}}$ defined by (21) is in a sense smaller than the corresponding restricted set when considering a slope constraint. In a similar sense, it is larger than the set $\tilde{\mathcal{H}}$ defined by (9). Vaguely speaking, one could say that this problem formulation fills some of the gap between the slope constraint formulation and the formulation with a finite dimensional set of designs. The filter radius $R$ determines the minimum width of the structural members, cf. (18) with $C_\infty = 3/(\pi R)$.

#### *7.2.1 Numerics and sensitivity analysis*

For the numerical procedure, the components of the discretized kernel $\phi^h$ are chosen similar to (20) where $c_i$ is independent of $i$ and $e_i$ may denote elements outside $\Omega$. However, because of the choice of filter kernel, the discretized design-to-density mapping is the summation over the elements that are within a distance of $R$ from $\Omega$,

$$\rho_j^h = \sum_{i=1}^{M^h} \xi_i^h \phi_{ji}^h,$$

hence summing from 1 to $M^h$ instead of to $N^h$. The sensitivities of the involved functions with respect to the design variable $\xi^h$ are now obtained by combining the corresponding sensitivities with respect to $\rho^h$ in section 4.3 and

$$\frac{\partial \rho_j^h}{\partial \xi_i^h} = \phi_{ji}^h.$$

### *7.2.2 Numerical results*

Two numerical examples have been chosen for this filter method, the MBB beam and the inverter mechanism. For the first example, the choice of material interpolation function is briefly discussed. It is experienced that interpolating with (5) could result in gray in regions in the structural domain where it is expected that the density should vanish, see for instance the center of solution $M_2$ in Figure 11. On the other hand, interpolating with (4) could result in gray where full density is expected, an effect that can be seen at the inner corners of the solution in Figure 13. These are consequences of the choice of material interpolation function and the functions in (4) and (5) are therefore combined to form a two-parameter material interpolation function according to

$$f_{q_1,q_2}(\rho) = \frac{\rho^{q_1}}{1 + (q_2 - 1)(1 - \rho)}.$$

Two MBB beam solutions for this material interpolation function are shown in Figure 15 where $q_1 = 1.5$ and $q_2 = 1.75$ for the first and $q_1 = 1.5$ and $q_2 = 3$ for the second solution. The filter radius is $R = 0.05$ and $R = 0.1$ for the two different examples respectively and the effects that are connected to the two individual material interpolation functions, (4) and (5), are eliminated. Worth mentioning is also that the numerical value of the maximal slope for each of the two solutions is almost identical to the corresponding theoretically obtained estimate in (23).

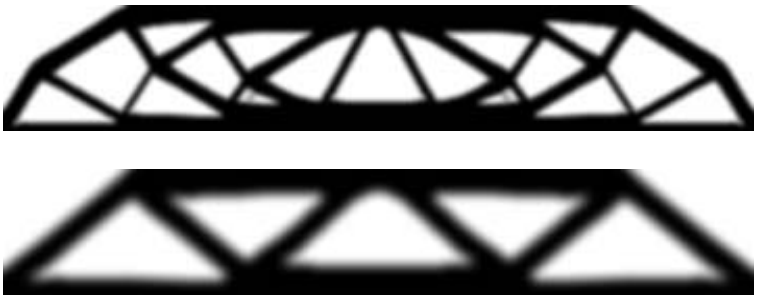

**Figure 15.** The MBB beam ($M_6 - M_7$) with a filtered design

The inverter mechanism is solved for $R = 0.05$ and $R = 0.1$ with the solutions shown in Figure 16. The material interpolation function is (5) with $q = 6$. The solutions here are very similar to the ones obtained with a finite dimensional set of designs in Figure 7, even the gray density region in solution $I_5$ is noticed. The appearance of this gray region in this case is the choice of a large filter radius and it is removed by solving the problem for a smaller filter radius, see solution $I_4$. From the discussion above, another suggestion to remove the gray in either one of the solutions $I_2$ or $I_5$ could be to change the material interpolation function from (5) to (4). The obvious difference between the solutions in Figure 7 and the ones in Figure 16 is that the structural members in the latter case are straight (and not jagged) regardless of the orientation in space. This is of course a consequence of only having a finitely number of design variables in the former case. With the exception of this difference, the relation $R = 1.5H$ seems to yield similar solutions for the two restriction methods. Common with these two restriction methods is that lumped compliance regions are explicitely excluded since the structural members are of a minimum width. This width is determined from the size of the gaussian bells in the case of a finite dimensional set of designs and the size of the filter radius in the case of a filtered design.

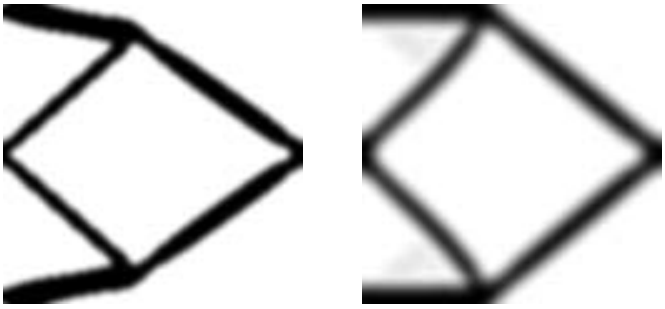

**Figure 16.** The inverter mechanism ($I_4 - I_5$) with a filtered design

### 7.3 Regularized Penalty

The last restriction method that is considered differs slightly in approach in comparison to the other methods. Instead of making an ill-posed problem well-posed by compactifying the feasible set, a well-posed problem is kept well-posed by making sure that all the involved functions are sufficiently regular. The starting problem is the variable thickness sheet problem, see section 2.4, and a penalty is added in the objective. Choosing this penalty as in (6) would make the problem ill-posed, hence the following penalty function is chosen. Compose the penalty function $g : L^2(\boldsymbol{R}^2) \to \boldsymbol{R}$

$$g(\tilde{\rho}) = \int_{\boldsymbol{R}^2} (1 - \tilde{\rho})(\tilde{\rho} - \rho_\epsilon)$$

and the filter operator $S : L^2(\Omega) \to L^2(\boldsymbol{R}^2)$

$$S(\rho) = \int_\Omega \rho(\boldsymbol{y})\phi(\cdot, \boldsymbol{y})d\boldsymbol{y}$$

where $\phi$ is given by (22). The continuity of $g$ and the compactness of $S$ makes the penalty function $P = g \circ S$ sufficiently regular in order to keep a well-posed problem. In [60] it is demonstrated that an almost discrete valued optimal design can be expected for a sufficiently high penalty coefficient $Q$ which also is illustrated in [61] where the method is extended to 3-dimensional topology optimization. Since this approach is based on starting from a well-posed problem, the theory fails for compliant mechanisms which is unfortunate.

#### *7.3.1 Numerics and sensitivity analysis*

The numerics are very similar to the ones in section 7.2.1 except for some details. For instance, the numerical calculation of $S$ can be written

$$\tilde{\rho}_i^h = \sum_{j=1}^{N^h} \rho_j^h \phi_{ij}^h$$

where $i$ may denote elements outside of $\Omega$. The penalty function $g$ is then applied to the elementwise constant function $\tilde{\rho}^h$,

$$g(\tilde{\rho}^h) = \sum_{i=1}^{M^h} m_i^h (1 - \tilde{\rho}_i^h)(\tilde{\rho}_i^h - \rho_\epsilon).$$

The sensitivities of the approximate penalty function with respect to $\rho^h$ are then obtained by combining the sensitivities of $S$ and $g$

$$\frac{\partial g}{\partial \tilde{\rho}_i^h} = m_i^h(1 + \rho_\epsilon - 2\tilde{\rho}_i^h)$$
$$\frac{\partial \tilde{\rho}_i^h}{\partial \rho_j^h} = \phi_{ij}^h.$$

### *7.3.2 Numerical results*

The cantilever beam is chosen to illustrate the features of regularized penalty approach. The filter radius is $R = 0.1$ and the solution is shown in Figure 17. The regularized penalty value is 0.21 obtained for a $Q$ value of $1.5 \cdot 10^{-2}$. The boundary description is very sharp as for perimeter constrained topology optimization. In fact, this approach is very similar to the perimeter approach since for a discrete valued solution, the contribution to the regularized penalty comes from a ribbon along the boundary of the structure. That is, the value of the penalty function is approximately proportional to the perimeter of the structure. That this is true is illustrated by the fact that the solution in Figure 17 is slightly better than solution $C_5$ in Figure 9 in the sense that both compliance and perimeter have lower values. Hence, solution $C_5$ in Figure 9 is a local optimum which again illustrates the difficulties with perimeter constrained topology optimization. Although the topologies of the two solutions are the same, a small difference in shape is present. An explanation of this could be that for a perimeter constraint, any change in shape of the boundary will most often result in an increase in compliance due to the penalty factor $q > 1$ in the material interpolation function. From this point of view, the regularized penalty approach allows for a more stable optimization procedure. As mentioned above, a crucial disadvantage with this approach is that the regularized penalty function does not have the compactness properties that the total variation possesses. Another problem is how to choose a suitable value of the penalty coefficient $Q$ for a general problem. One way of dealing with this problem is to use a continuation approach where the parameter $Q$ is gradually increased until a discrete valued solution is obtained, see [61].

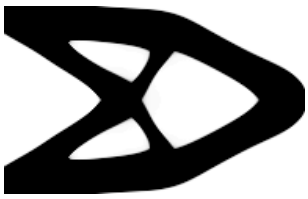

**Figure 17.** The cantilever beam ($C_6$) with a regularized penalty

Regarding the problem of designing a compliant mechanism, it is experienced that it is hard to develop a general strategy to treat this problem numerically. Based on this experience and the fact that the problem formulation is ill-posed, such a treatment is omitted.

## 8 OTHER RESTRICTION METHODS

The study in this paper is emphasised on methods for which a well-posed optimization problem can be posed but there are some other approaches that would have to fall in the category of a restriction method and hence should be mentioned in this context.

In Eschenauer *et al.* [62] the problem is not formulated in terms of distributing material in a fixed domain but the approach is based on solving a sequence of shape optimization

problems. After a shape optimization problem is solved, the topology of the structure is changed by introducing a small hole, called a bubble. The position of this bubble is determined from the solution of a variational problem and its boundary is allowed to change in the subsequent shape optimization problem. The procedure is terminated according to some suitable stopping criterion, for instance when a certain number of holes in the structure are present.

Xie and Steven [63] take another approach where the structure should follow an evolutionary path along which it is adapted to the environment it finds itself in. The goal is to evolve towards a fully stressed design starting from an initial configuration by removing material that is not effectively used. To determine the regions in the structure where material should be removed between each iteration, the stresses in the structure are measured. At points where the stress is low, the material is removed. This procedure is repeated until all stresses in the structure are within some percentage of the maximal stress.

Guedes and Taylor [64] and Rodrigues *et al.* [65] solves a sequence of convex optimization problems in which the volume constraint is weighted by a unit relative cost factor. This factor is systematically updated in order to encourage a clear material-void structure. In these references, the optimization is over a subset of all material tensors, see [13, 66], but a similar approach can be applied on the variable thickness sheet problem [67].

In signal and image processing, wavelets have made an impact the last 15 years. The advantage with wavelet methods in comparison to traditional fourier methods is that wavelets have an ability to represent discontinuities efficiently. Kim and Yoon [68] points out that this makes the use of wavelets in topology optimization suitable. They perform the optimization in wavelet space and the density is determined from the (inverse) wavelet transform. A very similar approach is taken by Poulsen [69] with the exception that wavelet techniques are used mainly to suppress checkerboards. He also suggests how to obtain a well-posed optimization formulation by using only the wavelet coefficients corresponding to the coarsest scales to determine the density, an approach that is very similar to a finite dimensional set of designs. It is shown with aid of the Haar wavelet that the numerical examples are not prone to numerical instabilities such as mesh-dependence or checkerboards.

## 9 DISCUSSION AND CONCLUSIONS

This paper deals with restriction methods in topology optimization of elastic continua, a measure for obtaining well-posed problem formulations. The problems of designing for maximum stiffness and designing compliant mechanisms in linear elasticity are treated. A number of restriction methods are discussed both from a theoretical and a numerical point of view and various advantages and drawbacks are mentioned. It is indicated how some of the different restriction methods can be ordered with respect to the size of their corresponding set of admissible densities $\tilde{\mathcal{H}}$. A perimeter constraint determines a large $\tilde{\mathcal{H}}$ while a finite dimensional set of designs determines a small $\tilde{\mathcal{H}}$. Starting from the smallest set of admissible densities, the suggested ordering would be

- Finite dimensional set of designs
- Filtering the design
- Slope constraint
- $\boldsymbol{L}^p$-constraint
- Perimeter constraint

From a theoretical point of view, this ordering corresponds to the methods ability of finding a reasonable optimal structure. For a small $\tilde{\mathcal{H}}$ this structure is in general characterized by a blurry boundary description and perhaps even jagged structural members. On the other hand, for a large $\tilde{\mathcal{H}}$ the optimal structure can have a very sharp and nice boundary description as with for instance a perimeter constraint. If the set of densities is too large, there may be theoretical problems as it may lack compactness properties that are required for well-posedness. This happens if no (or weak) compactifying constraints are imposed, see section 7.3. From a numerical point of view, there are advantages with a small $\tilde{\mathcal{H}}$ since this in general yield a faster and more stable optimization procedure, see appendix B. This knowledge should be a considerable help when choosing an appropriate restriction method in topology optimization. The first two restriction methods, finite dimensional set of designs and filtering the design, are considered most attractive as they are non-sensitive to local optima and yield easily interpretable results.

The numerical examples are solved with a strict termination criterion and the material interpolation function is in most cases chosen as (5) with $q = 6$. The reason for the latter is that the other penalty schemes in section 2.3 result in problems that appear more sensitive to local optima and $q = 6$ is in general an appropriate value of the penalty parameter. When a fine topology is desired the penalty can be weakened, see solutions $C_4$, $M_1$ and $M_6$, and in such a case a strict convergence criterion is necessary since otherwise the optimization procedure terminates too early.

A fundamental issue that has been postponed up to now is how to interpret a numerical result. Let an optimal density to a problem be denoted $\rho^*$. The interpretation is straightforward when the solution is discrete valued but may be ambiguous when there are regions of intermediate density values in the structural domain. One obvious choice would be to post-process the result by for instance choosing a cut-off density $\rho_c$ and determining a discrete valued solution $\tilde{\rho}^*$ through

$$\tilde{\rho}^*(\boldsymbol{x}) = \begin{cases} \rho_\epsilon & \text{if } \rho^*(\boldsymbol{x}) < \rho_c \\ 1 & \text{otherwise} \end{cases}$$

where $\rho_c$ is chosen so that

$$\int_\Omega (\rho^* - \tilde{\rho}^*) = 0.$$

There is no guarantee however, that the solution $\tilde{\rho}^*$ is good even when $\rho^*$ in some sense is. Nevertheless, for any the restriction methods in this paper there is reason to believe that such an operation will only slightly change the structural behaviour since the intermediate density values are most often representing transition zones between full density and void. If it for some reason is important not to change the optimal density $\rho^*$, it would have to be interpreted as the density of an isotropic material with an effective stiffness represented by the tensor $\boldsymbol{E}_q(\rho^*)$. This can only be possible if the material interpolation function is chosen so that the Hashin-Shtrikman bounds [70] are not violated. For the two material interpolation functions (4) and (5), this means that the parameter $q$ has to be chosen sufficiently large, see [29, 32]. The intention with the restriction methods in this paper is however to interpret a solution as a suggestion for a solid-void structure and hence the former approach is to prefer. In table 1 in appendix A, the two structural related functions are evaluated for $\rho^*$, $f_q(\rho^*)$ as well as for $\tilde{\rho}^*$ for the purpose of comparing the three values. The value that is obtained for $f_q(\rho^*)$ differs in general much from the other two, a difference that is closely connected to the amount of gray in the solution $\rho^*$, see table 1. Even though the values for $\rho^*$ and $\tilde{\rho}^*$ are different, they are in general close enough to conclude that restriction can advantagously be used for designing stiff structures as well as compliant mechanisms.

## A CKNOWLEDGEMENTS

This w ork is financially supported by the National Net work in Applied Mathematics (NTM) and the National Graduate School in Scientific Computing (NGSSC). The author wishes to thank Dr. Joakim Petersson for valuable discussions both before and during the preparation of this paper. Another ac knowledgemen t goes to Dr. Krister Svanberg for providing the MMA-code and for discussing various implementation aspects regarding this code.

## REFERENCES

1 M.P . Bendsøe (1995), *Optimization of Structur al Topology, Shape and Material*, Springer-Verlag, Berlin.

2 B. Hassani and E. Hin ton (1999), *Homogenization and Structural Topology Optimization: Theory, Practice and Software*, Springer-Verlag, London Limited.

3 G.I.N. Rozvany, M.P . Bendsøe and U. Kirsc h (1995), "Layout optimization of structures", *Appl. Mech. Rev.*, **48**, 41–119.

4 M.P . Bendsøe and N. Kikuc hi (1988), "Generating optimal topologies in structural design using a homogenization method", *Comput. Methods Appl. Me ch. Eng.*, **71**, 197–224.

5 R.V. Kohn and G. Strang (1986), "Optimal design and relaxation of variational problems", *Comm. Pure Appl. Math.*, **39**, 113–137 (Part I), 139–182 (Part II) and 353–377 (Part III).

6 S. Spagnolo (1976), "Convergence in energy for elliptic operators", in: B. Hubbard (Ed.), *Numeric al Solutions of Partial Differ ential Equations III*, Academic Press, 469–498.

7 K.A. Lurie and A.V. Cherkaev (1997), "Effective characteristics of composite materials and the optimal design of structural elements", *Topics in the Mathematic al Mo delling of Comp osite Materials*, in A. Cherkaev and R. K ohn (Eds.), Birkhäuser Boston, 175–258.

8 G. Allaire and R.V. Kohn (1993), "Optimal design for minimum weight and compliance in plane stress using extremal microstructures", *Europ. J. Me ch. A. Solids*, **12:6**, 838–878.

9 M.P . Bendsøe, A. Díaz and N. Kikuchi (1993), "Topology and generalized layout optimization of elastic structures", *Topology Design of Structures*, in M.P . Bendsøe and C.A. Mota Soares (Eds.), Klu wer Academic Publishers, 159–205.

10 G. Allaire, E. Bonnetier, G. Francfort and F. Jouve (1997), "Shape optimization by the homogenization method", *Numer. Math.*, **76**, 27–68.

11 G. Allaire and R.V. Kohn (1993), "Optimal bounds on the effective behaviour of a mixture of two well-ordered materials", *Q. Appl. Math. LI*, **4**, 675–699.

12 J. Petersson (1996), "On stiffness maximization of variable thickness sheet with unilateral contact", *Q. Appl. Math.*, **54**, 541–550.

13 M.P. Bendsøe, J.P. Guedes, R.B. Haber, P. Pedersen and J.E. Taylor (1994), "An analytical model to predict optimal material properties in the context of optimal structural design", *J. Applied Mech.*, **61**, 930–937.

14 K. Yuge, N. Iw ai and N. Kikuc hi (1999), "Optimization of 2-D structures subjected to nonlinear deformations using the homogenization method", *Struct. Optim.*, **17**, 286–299.

15 T. Buhl, C.B.W. Pedersen and O. Sigm und (2000), "Stiffness design of geometrically non-linear structures using topology optimization", *Struct. Optim.*, **19:2**, 93–104.

16 K. Maute, S. Sc hwartz and E. Ramm (1998), "Adaptive topology optimization of elastoplastic structures", *Struct. Optim.*, **15**, 81–91.

17 G.K. Ananthasuresh, S. Kota and N. Kikuchi (1994), "Strategies for systematic synthesis of compliant MEMS", *1994 ASME Winter Annual Meeting* DSC-Vol. **55-2**, 677–686.

18 G.K. Ananthasuresh and S. Kota (1995), "Designing compliant mechanisms", *Mech. Eng*, **117** **11**, 93–96.

19 M.I. Frecker, G.K. Ananthasuresh, S. Nishiwaki, N. Kikuchi and S. Kota (1997), "Topological synthesis of compliant mechanisms using multi-criteria optimization", *Trans. ASME, J. Mech. Des.*, **119**, 238–245.

20 S. Nishiwaki, M.I. Frecker, S. Min and N. Kikuchi (1998), "Topology optimization of compliant mechanisms using the homogenization method", *Int. J. Numer. Methods Eng.*, **42**, 535–559.

21 J.A. Hetrick and S. Kota (1999), "An energy formulation for parametric size and shape optimization of compliant mechanisms", *Trans. ASME, J. Mech. Des.*, **121**, 229–234.

22 U.D. Larsen, O. Sigmund and S. Bouwstra (1997), "Design and fabrication of compliant micromechanisms and structures with negative poisson's ratio", *J. Microelectromech. Syst.*, **6:2**, 99–106.

23 O. Sigmund (1997), "On the design of compliant mechanisms using topology optimization", *Mech. Struct. Mach.*, **25**, 493–524.

24 Claus B.W. Pedersen, Thomas Buhl and Ole Sigmund (2001), "Topology synthesis of large-displacement compliant mechanisms", *Int. J. Numer. Methods Eng.*, **50**, 2683–2705.

25 T.E. Bruns and D.A. Tortorelli (2001), "Topology optimization of nonlinear elastic structures and compliant mechanisms", *Comput. Methods Appl. Mech. Eng.*, **190**, 3443–3459.

26 R.A. Adams (1975), *Sobolev Spaces*, Academic Press, New York.

27 M.P. Bendsøe (1989), "Optimal shape design as a material distribution problem", *Struct. Optim.*, **1**, 193–202.

28 M. Zhou and G.I.N. Rozvany (1991), "The COC algorithm, part II: topological, geometrical and generalized shape optimization", *Comput. Methods Appl. Mech. Eng.* **89**, 309–336.

29 M. Stolpe and K. Svanberg (2001), "An alternative interpolation scheme for minimum compliance topology optimization", Optimization and Systems Theory, Royal Institute of Technology, Report TRITA/MAT-00-OS13. To appear in *Struct. Multidisc. Optim.*

30 K. Maute and E. Ramm (1995), "Adaptive topology optimization", *Struct. Optim.*, **10**, 100–112.

31 H.P. Mlejnek and R. Schirrmacher (1993), "An engineer's approach to optimal distribution and shape finding", *Comput. Methods Appl. Mech. Eng.*, **106**, 1–26.

32 M.P. Bendsøe and O. Sigmund (1999), "Material interpolation schemes in topology optimization", *Arch. Appl. Mech.* **69**, 635–654.

33 C.S. Jog and R.B. Haber (1996), "Stability of finite element models for distributed-parameter optimization and topology design", *Comput. Methods Appl. Mech. Eng.*, **130**, 203–226.

34 G. Allaire and R.V. Kohn (1993), "Topology optimization and optimal shape design using homogenization", *Topology Design of Structures*, in M.P. Bendsøe and C.A. Mota Soares (Eds.), Kluwer Academic Publishers, 207–218.

35 M.P. Rossow and J.E. Taylor (1973), "A finite element method for the optimal design of variable thickness sheets", *AIAA Journal*, **11**, 1566–1568.

36 J. Céa and K. Malanowski (1970), "An example of a max-min problem in partial differential equations", *SIAM J. Control* **8:3**, 305–316.

37 K. Svanberg (1987), "The method of moving asymptotes - a new method for structural optimization", *Int. J. Numer. Methods Eng.*, **24**, 359–373.

38 J. Petersson and O. Sigmund (1998), "Slope constrained topology optimization", *Int. J. Numer. Methods Eng.*, **41**, 1417–1434.

39 M. Stolpe and K. Svanberg (2001), "On the trajectories of penalization methods for topology optimization", *Optimization and Systems Theory*, Royal Institute of Technology, Report TRITA/MAT-00-OS02. *Struct. Multidisc. Optim.*, **21**, **2**, 128–139.

40 A. Díaz and O. Sigmund (1995), "Checkerboard patterns in layout optimization", *Struct. Optim.*, **10**, 40–45.

41 O. Sigmund and J. Petersson (1998), "Numerical instabilities in topology optimization: A survey on procedures dealing with checkerboards, mesh-dependencies and local minima", *Struct. Optim.*, **16**, 68–75.

42 V. Maz'ya (1994), "Approximate approximations", *The Mathematics of Finite Elements and Applications*, in J.R. Whiteman (Ed.), John Wiley & Sons Ltd, 77–104.

43 R. Temam (1985), *Mathematical Problems in Plasticity*, BORDAS, Paris.

44 E. Giusti (1984), *Minimal Surfaces and Functions of Bounded Variation*, Birkhäuser Boston, Inc.

45 L. Ambrosio and G. Butazzo (1993), "An optimal design problem with perimeter penalization", *Calc. Var.*, **1**, 55–69.

46 J. Petersson (1999), "Some convergence results in perimeter-controlled topology optimization", *Comput. Methods Appl. Mech. Eng.*, **171**, 123–140.

47 R.B. Haber, C.S. Jog and M.P. Bendsøe (1996), "A new approach to variable-topology shape design using a constraint on perimeter", *Struct. Optim.*, **11**, 1–12.

48 P. Duysinx (1997), "Layout optimization: A mathematical programming approach", DCAMM Report 540, Technical University of Denmark.

49 M. Beckers (1999), "Topology optimization using a dual method with discrete variables", *Struct. Optim.*, **17**, 14–24.

50 P. Fernandez, J.M. Guedes and H. Rodrigues (1999), "Topology optimization of three-dimensional linear elastic structures with a constraint on *perimeter*", *Comput. Struct.*, **73**, 583–594.

51 J. Petersson, M. Beckers and P. Duysinx (1999), "Almost isotropic perimeters in topology optimization: Theoretical and numerical aspects", in C.L. Bloebaum, K.E. Lewis and R.W. Mayne (Eds.), WCSMO-3, Proceedings of the *Third World Congress of Structural and Multidisciplinary Optimization*, 117–119.

52 M.P. Bendsøe (1983-84), "On obtaining a solution to optimization problems for solid, elastic plates by restriction of the design space", *J. Struct. Mech*, **11**(**4**), 501–522.

53 F. Niordson (1983), "Optimal design of elastic plates with a constraint on the slope of the thickness function", *Int. J. Solids Struct.*, **19**, 141–151.

54 I. Hlaváček, I. Bock and J. Lovišek (1985), "Optimal control of a variational inequality with applications to structural analysis. II. Local optimization of the stress in a beam. III. Optimal design of an elastic plate", *Appl. Math. Optim.*, **13**, 117–136.

55 M. Zhou, Y.K. Shyy and H.L. Thomas (1999), "Checkerboard and minimum member size control in topology optimization", in C.L. Bloebaum, K.E. Lewis and R.W. Mayne (Eds.), WCSMO-3, Proceedings of the *Third World Congress of Structural and Multidisciplinary Optimization*, 440–442.

56 O. Sigmund (1994), *Design of material structures using topology optimization*, Ph.D. thesis, DCAMM, Technical University of Denmark.

57 O. Sigmund and T. Buhl (2000), "Design of multiphysics actuators using topology optimization", DCAMM Report 632, Technical University of Denmark. To appear in *Comput. Methods Appl., Mech. Eng.*

58 N.L. Pedersen (2000), "Maximization of eigenvalues using topology optimization", *Struct. Multidisc. Optim.*, **20**, 2–11.

59 B. Bourdin (1999), "Filters in topology optimization", DCAMM Report 627, Technical University of Denmark. To appear in *Int. J. Numer. Methods Eng.*

60 T. Borrvall and J. Petersson (2001), "Topology optimization using regularized intermediate density control", *Comput. Methods Appl. Mech. Eng.*, **190**, 4911–4928. Department of Mechanical Engineering, Linköping University, LiTH-IKP-R-1086.

61 T. Borrvall and J. Petersson (2000), "Large scale topology optimization in 3D using parallel computing", Department of Mechanical Engineering, Linköping University, LiTH-IKP-R-1130. To appear in *Comput. Methods Appl. Mech. Eng*

62 H.A. Eschenauer, V. Kobelev and A. Schumacher (1994), "Bubble method of topology and shape optimization of structures", *Struct. Optim.*, **8**, 42–51.

63 Y.M. Xie and G.P. Steven (1993), "A simple evolutionary procedure for structural optimization", *Comput. Struct.*, **49**, 885–896.

64 J.M. Guedes and J.E. Taylor (1997), "On the prediction of material properties and topology optimization for optimal continuum structures", *Struct. Optim.*, **14**, 193–199.

65 H. Rodrigues, C.A. Soto and J.E. Taylor (1999), "A design model to predict optimal two-material composite structures", *Struct. Optim.*, **17**, 186-198.

66 U.T. Ringertz (1993), "On finding the optimal distribution of material properties", *Struct. Optim.*, **5**, 265–267.

67 M. Torabzadeh-Tari (1999), "Implementation of a topology optimization approach in TRINITAS: a new weight function in the volume constraint", Department of Mechanical Engineering, Linköping University, LiTH-IKP-Ex-1584.

68 Y.Y. Kim and G.H. Yoon (2000), "Multi-resolution multi-scale topology optimization - a new paradigm", *Int. J. Solids Struct.*, **37**, 5529–5559.

69 T. Poulsen (2000), "Topology optimization in wavelet space", DCAMM Report 639, Technical University of Denmark.

70 Z. Hashin and S. Shtrikman (1963), "A variational approach to the theory of the elastic behaviour of multiphase materials", *J. Mech. Phys. Solids*, **11**, 127–140.

Please address your comments or questions on this paper to:
International Center for Numerical Methods in Engineering
Edificio C-1, Campus Norte UPC
Grand Capitán s/n
08034 Barcelona, Spain
Phone: 34-93-4106035; Fax: 34-93-4016517
E-mail: onate@cimne.upc.es

## A COMPUTATIONAL DATA

This appendix presents a Table containing the computational data for the numerical examples in this paper. The entries in the table are the following. The names of the numerical examples are given in the column "Ex." and corresponds to identical names in the figure texts throughout the paper. For each example, half of the structural domain is discretized into a mesh of "Mesh" finite elements. The optimal structure has a compliance of "Compl." and exerts a force of "Force" onto a workpiece. Each of these entries contains the following three values. The first corresponds to the structure that can be represented by the optimal density $\rho^*$, the second value is for the structure represented by $f_q(\rho^*)$, i.e. the "true" optimal structure, and the third value is for a post-processed structure $\tilde{\rho}^*$ obtained as in section 9. The amount of intermediate density values is given in the column "Pen." by

$$100\frac{P(\rho^*)}{P_{\max}},$$

where $P$ is given by (6). $P_{\max}$ is the maximum possible value of this penalty function which is attained for a completely gray density, $\rho = \min(0.5(1+\rho_\epsilon), \overline{V}/|\Omega|)$. The last column, "Iter.", gives the number of optimization iterations required to reach the optimal solution starting from a constant density, $\rho = \overline{V}/|\Omega|$. A limit of maximum 10000 iterations is used.

| Ex. | Mesh | Compl. ($\times 10^{-2}$) | Force | Pen. (%) | Iter. |
|---|---|---|---|---|---|
| $C_1$ | $10 \times 32$ | 3.62/4.90/3.97 | $-/-/-$ | 31.1 | 92 |
| $C_2$ | $20 \times 64$ | 3.56/4.84/3.74 | $-/-/-$ | 30.5 | 225 |
| $C_3$ | $60 \times 192$ | 3.57/4.86/3.72 | $-/-/-$ | 30.5 | 292 |
| $C_4$ | $60 \times 192$ | 3.54/3.57/3.57 | $-/-/-$ | 1.7 | 1503 |
| $C_5$ | $60 \times 192$ | 3.66/3.66/3.67 | $-/-/-$ | 0.0 | 10000 |
| $C_6$ | $60 \times 192$ | 3.57/3.57/3.62 | $-/-/-$ | 3.5 | 1989 |
| $M_1$ | $60 \times 180$ | 8.52/8.72/8.67 | $-/-/-$ | 7.4 | 10000 |
| $M_2$ | $60 \times 180$ | 8.93/9.99/9.16 | $-/-/-$ | 17.4 | 4571 |
| $M_3$ | $60 \times 180$ | 8.81/10.68/9.21 | $-/-/-$ | 27.1 | 4963 |
| $M_4$ | $60 \times 180$ | 8.67/11.77/9.30 | $-/-/-$ | 39.6 | 4675 |
| $M_5$ | $60 \times 180$ | 8.90/10.22/9.12 | $-/-/-$ | 21.8 | 566 |
| $M_6$ | $60 \times 180$ | 8.54/9.26/8.72 | $-/-/-$ | 21.5 | 3283 |
| $M_7$ | $60 \times 180$ | 9.00/10.91/9.16 | $-/-/-$ | 26.7 | 1812 |
| $I_1$ | $60 \times 120$ | 5.91/10.00/6.73 | 1.31/1.52/1.48 | 24.5 | 1100 |
| $I_2$ | $60 \times 120$ | 3.95/10.00/5.39 | 0.80/0.96/1.09 | 46.2 | 310 |
| $I_3$ | $60 \times 120$ | 9.75/10.00/9.88 | 2.02/2.04/2.03 | 1.6 | 1422 |
| $I_4$ | $60 \times 120$ | 6.73/10.00/7.31 | 1.51/1.71/1.65 | 20.5 | 4090 |
| $I_5$ | $60 \times 120$ | 4.70/10.00/5.56 | 1.01/1.15/1.22 | 40.0 | 2518 |
| $G_1$ | $30 \times 60$ | 9.58/10.00/17.73 | 1.81/1.83/1.77 | 2.0 | 878 |
| $G_2$ | $60 \times 120$ | 9.94/10.00/10.04 | 1.90/1.90/1.90 | 0.4 | 1253 |
| $G_3$ | $90 \times 180$ | 9.88/10.00/10.01 | 1.91/1.92/1.92 | 0.8 | 2078 |
| $G_4$ | $30 \times 60$ | 7.34/10.00/8.24 | 1.50/1.51/1.51 | 28.4 | 309 |
| $G_5$ | $60 \times 120$ | 7.37/10.00/7.95 | 1.52/1.58/1.55 | 23.2 | 1342 |
| $G_6$ | $90 \times 180$ | 7.26/10.00/7.80 | 1.50/1.60/1.56 | 21.6 | 3154 |

**Table 1.** Computational data for the numerical examples

## B COMPARISON OF THREE RESTRICTION METHODS

This appendix is dev oted to a comparison of three t ypes of restriction methods for compliance minimization. The three types are finite dimensional set of designs (gaussian bells), a filter method (filtering the design) and a bound on the design gradient ($\boldsymbol{L}^2$-constraint). The comparison is from a more practical point of view as the optimization procedure for each of the examples in this appendix is terminated when the relative difference bet w een tw o successive objective functions is less than $10^{-6}$. This convergence criterion is less strict than the one for the examples in the paper and is more suitable for demonstrating the convergence properties of the methods. The cantilever beam and the MBB beam are solved with both (4) and (5) as the material interpolation function and the in volved parameters are chosen so that similar solutions for the differen t methods are obtained. The nmber of optimization iterations is reduced and in general, a smaller feasible set of densities yields a smaller n um ber of optimization iterations. F or compliant mechanism design, this weak criterion in general results in a too early termination. It is also seen in the Figures 18–21 how a larger set of densities allows for smooth optimal solutions with less amount of intermediate density values.

**Figure 18.** The cantilever beam with material in terpolation function (5) $q = 6$. The parameters $H = 1/15$, $R = 0.1$ and $\tilde{c}_2 = 5.0 \cdot 10^{-4}$ are used and the number of optimization iterations are 65,61 and 181 respectively

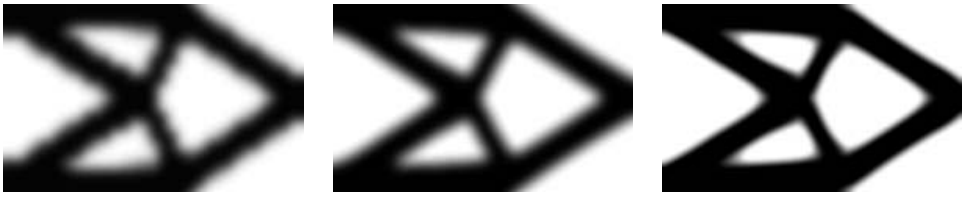

**Figure 19.** The cantilever beam with material in terpolation function (4) $q = 3$. The parameters $H = 1/10$, $R = 0.15$ and $\tilde{c}_2 = 7.5 \cdot 10^{-4}$ are used and the number of optimization iterations are 55,543 and 641 respectiv ely

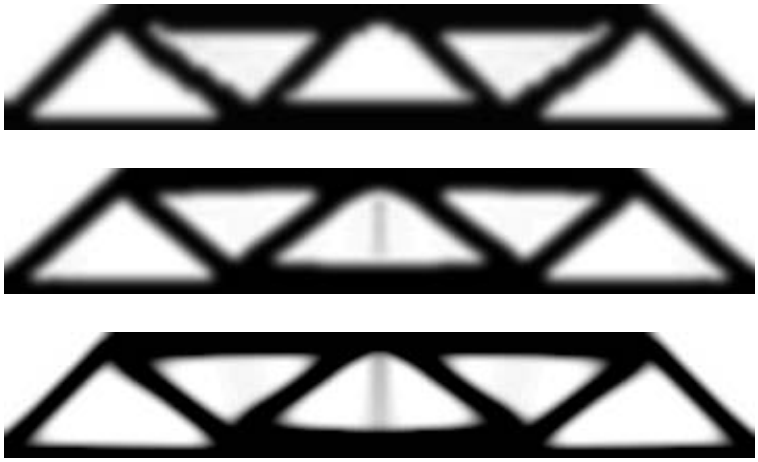

**Figure 20.** The MBB beam with material interpolation function (5), $q = 6$. The parameters $H = 1/15$, $R = 0.1$ and $\tilde{c}_2 = 5.6 \cdot 10^{-5}$ are used and the num ber of optimization iterations are 119,475 and 539 respectiv ely

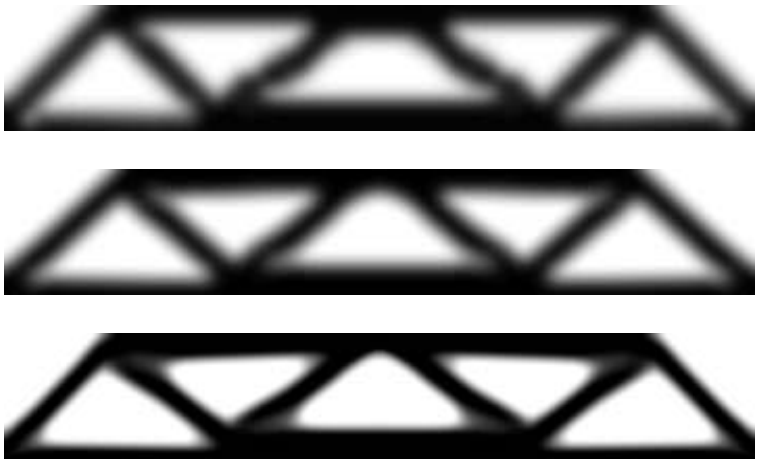

**Figure 21.** The MBB beam with material interpolation function (4), $q = 3$. The parameters $H = 1/10$, $R = 0.15$ and $\tilde{c}_2 = 8.3 \cdot 10^{-5}$ are used and the num ber of optimization iterations are 115,311 and 388 respectiv ely